An oil spill model for South African waters

Trajectory and fate analysis of deepwater blowout spill scenarios

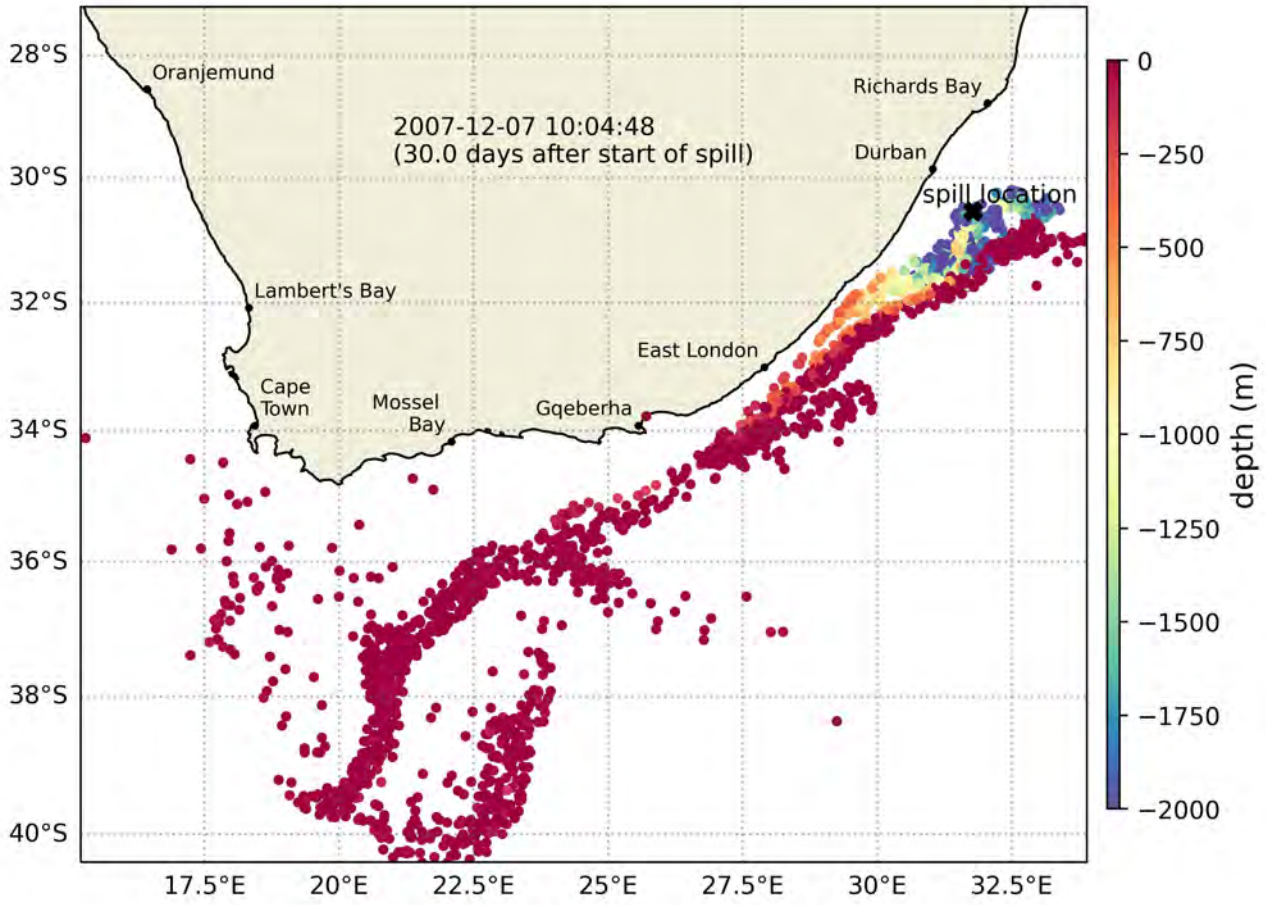

An oil spill model for South African waters

Trajectory and fate analysis of deepwater blowout spill scenarios

Giles Fearon[1], Rory Laing[2], Annalisa Bracco[3], and Danielle Reich[4]

[1]Department of Oceanography, University of Cape Town, South Africa
[2]Wildlands Conservation Trust (WILDTRUST), Pietermaritzburg, South Africa
[3]School of Earth and Atmospheric Sciences, Georgia Institute of Technology, Atlanta, United States
[4]Shoal's Edge Consulting, Florida, United States

Revision	Date	Author(s)	Description
01	12 May 2023	All	First draft

Summary

This report presents oil spill modelling undertaken to predict the trajectory and fate of oil released into the marine environment from potential blowout spill scenarios from proposed offshore oil exploration wells within South Africa's Exclusive Economic Zone (EEZ). We focus mainly on blowout spill scenarios off the east coast of South Africa, but also consider potential spills off the south and west coasts.

The transport and fate of oil from a blowout spill off the east coast of South Africa is shown to be largely dictated by the variability of the Agulhas Current, which can transport oil great distances. The oceanographic features of the region lead to strong connectivity between the deep-water spill location off the east coast of South Africa and the coastlines of Southern Africa, with most of the South African coastline being shown to be under at least some risk of impact from an east coast blowout spill.

The results of the oil spill modelling indicate that a 15 day blowout of light crude oil off the east coast of South Africa could have as much as a 79% chance of impacting the shoreline to the extent where beach clean-up operations would be required. Significant ecological shoreline impacts, which could result in mortality of seabirds and other wildlife associated with the shoreline, are predicted with a 55-58% probability of occurrence in the event of an east coast blowout spill (the range represents the uncertainty in the rise velocity of oil from the well). The median spatial extent of potential ecological impacts on the ocean surface is estimated to be between 60 000 and 280 000 km^2 (again, depending on the rise velocity of oil from the well).

Interestingly, the south coast of South Africa (Cape Town to Gqeberha) is at a higher risk of needing beach clean-up operations than the east coast (78% vs 43% for the faster rising droplet scenario), despite the location of the blowout spill being located off the east coast. This is attributed to the relative stability of the Agulhas Current along on the east coast, before becoming less intense but more variable south of Gqeberha, allowing oil to become entrained onto the Agulhas Bank where the predominant winds in the region aid in shoreline oiling. Indeed, the specific location with the greatest risk of requiring beach cleanup operations is Cape Agulhas, on the southern tip of the continent, with a 36% probability (for the fast rising droplet

scenario). The minimum time to shoreline impact from an east coast blowout spill could be as little as three days for the east coast of South Africa, increasing to about 10 days for the south coast and about 30 days for the west coast. The difficulty in predicting where oil will make landfall, along with the potentially small amount of time available for mobilisation, would provide significant challenges to a coordinated clean-up effort in the event of a spill off the east coast.

Sensitivity tests to both season and ocean model resolution indicate that, in general, processes which lead to enhanced entrainment of oil onto the Agulhas Bank lead to higher shoreline impacts on both the south and west coasts of South Africa. Summer tends to be associated with elevated easterly winds which increase shoreline impacts when compared with winter spills. Higher resolution ocean models include more entrainment of oil onto the Agulhas Bank through their inclusion of more sub-mesoscale variability in the form of cyclonic eddies along the inner edge of the Agulhas Current.

A comparison between blowout spills at different locations (east coast, south coast and west coast) unsurprisingly indicates that the different locations pose very different risks of impacts. Of the three considered locations, the south coast location results in the highest risk of shoreline impact, with an estimated 86% chance of a 15 day blowout requiring beach clean-up operations (under the faster rising droplet scenario).

The results of this study are intended to provide stakeholders with an independent assessment of the potential risks posed by deep-water blowout spills from offshore oil and gas exploration and extraction. It is furthermore intended that the oil spill model results presented here will be used in an assessment of environmental, social, and economic risks of major blowouts from drilling sites being pursued in South Africa, which is the topic of ongoing work.

Contents

1

Introduction

1.1. Background

At any given time, an average of 90% of the oceans within South Africa's Exclusive Economic Zone (EEZ) are under lease for oil and gas exploration or extraction. This is highlighted in Figure 1.1, which provides a summary of the offshore oil and gas exploration currently under way.

Oil and gas exploration and extraction introduces the risk of various types of spills into the marine environment, such as surface spills of marine diesel, accidental releases of Non Aqueous Drilling Fluid (NADF), and blowout spills at the wellhead on the seafloor. Blowout spills pose the greatest potential ecological risk, as evidenced by the Deepwater Horizon disaster in the Gulf of Mexico in 2010. The spill released over 4 million barrels of oil into the marine environment over 87 days, leading to extensive ecological impacts within the water column, on the water surface, on shorelines and on the seabed (Ainsworth et al., 2018; Berenshtein et al., 2020; Bracco et al., 2020). The potential impacts of similar blowout spills within South Africa's EEZ due to these activities therefore needs to be properly considered.

Applications for exploratory and extractive drilling rights by oil and gas companies are required to be subjected to an Environmental Impact Assessment (EIA) process. While the modelling of oil spills is a requirement of these studies, the potential economic benefits of oil production wells are deemed to outweigh the associated ecological risk, and as such applications are currently being approved. These assessments and approvals are however being objected to by many stakeholders, including non-governmental organizations (NGOs), coastal communities, and fishers. An obstacle to stakeholders in this push-back is the lack of an in-

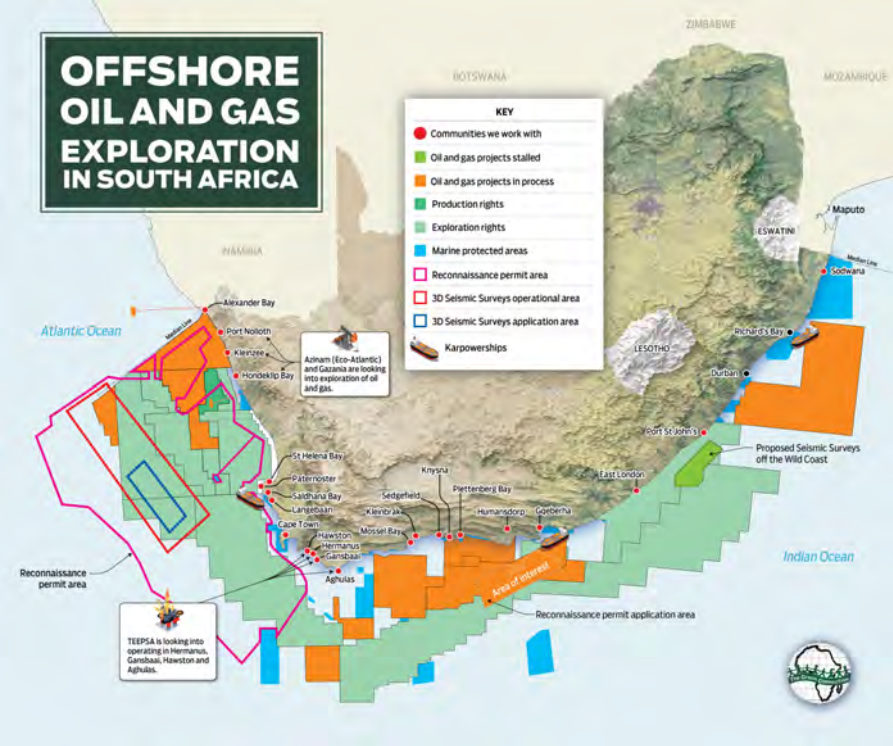

Figure 1.1: Map indicating the extent of offshore oil and gas exploration in South Africa's EEZ (`https://thegreenconnection.org.za/opposing-oil-and-gas-exploration/`).

dependent oil spill model which can be used as a benchmark for comparison against oil spill modelling undertaken by project proponents within the EIA's.

In this study, we present oil spill modelling undertaken to predict the trajectory and fate of oil released into the marine environment from potential blowout spill scenarios which may result from proposed offshore oil exploration wells within South Africa's EEZ. The model takes into account the complex and highly dynamic oceanographic features within South Africa's EEZ, and how oil from potential deep-water blowouts is likely to behave once released into this environment. The results of the study are intended to provide stakeholders and decision-makers with an independent assessment of the potential risks posed by deepwater blow-out spills from offshore oil exploration and extraction wells.

1.2. Study approach

One of the biggest challenges in modelling potential oil spills is to define credible spill scenarios, given that there are a functionally infinite number of possible combinations of spill volume, spill type, location, duration, season, and oil type. While most of South Africa's EEZ is cur-

rently being targeted by the oil and gas industry (Figure 1.1), this study considers only three potential spill locations, comprised of east, south and west coast spills, respectively. All three considered locations are coincident with regions which are currently being targeted by the oil and gas industry. The focus of the study is predominantly on the east coast location, while the other two locations are presented as sensitivity tests. We consider only blowout spill scenarios (as opposed to smaller marine diesel and NADF spills) as although these have a lower likelihood of occurrence, they pose the largest potential ecological impact (Etkin, 2015).

We simulate the defined spill scenarios using the OpenOil module of OpenDrift[1] (Dagestad et al., 2018), an open-source software package designed for modelling the trajectories and fate of objects or substances drifting in the ocean. A stochastic approach is followed, whereby each spill scenario is modelled 200 times, generating an ensemble of deterministic simulations, each varying only in the hypothetical start date of the simulation. The ensemble of deterministic simulations are evaluated statistically to provide insight into the probable behaviour of blowout spills in response to the varying environmental conditions (i.e. ocean currents and winds) over the study area.

1.3. Layout of the report

Given the importance of the prevailing ocean currents and winds on the ultimate fate of oil spills, Section 2 provides an assessment of selected environmental datasets providing these inputs to the oil spill model. Section 3 provides the rationale for selecting the oil spill scenarios, describes the configuration of the OpenOil model and details how the model outputs were processed. The results of the simulations are provided in Section 4, while the results are discussed and conclusions drawn in Section 5.

[1] https://github.com/OpenDrift/opendrift/

2

Environmental data

2.1. Introduction

Oil released into the marine environment is transported by the prevailing ocean currents and also by winds when floating on the surface of the ocean. Wind also influences the characteristics of oil on the surface through its influence on weathering processes such as evaporation, emulsification and dispersion (French-McCay, 2004) and can be a dominant driver of surface oil movement (Gurumoorthi et al., 2021). Ocean currents would tend to dominate oil advection in highly energetic and turbulent environments such as in western boundary currents, as is considered in this study. An accurate representation of the spatial and temporal variability of these environmental forces is therefore of great importance for simulating the transport, weathering and ultimate fate of oil spills. This section provides a brief description of the environmental data that were used as input to the oil spill model and compares these data against selected in-situ and satellite observations. The presented data are used to provide the meteorological and oceanographic context for the region of interest.

2.2. Description of datasets

2.2.1. GLORYS

Global ocean and atmospheric reanalysis products are commonly adopted as environmental input to oil spill models. These model simulations are assimilated with available in-situ and satellite observations in an attempt to improve model accuracy. A number of freely available global ocean reanalysis products exist, including the CSIRO's Bluelink Reanalysis (BRAN), FNMOC's Reanalyis (HYCOM) and Mercator Ocean's Global Reanalysis (GLORYS). In a re-

cent assessment of these three reanalysis products, specifically focused on their ability to represent the oceanographic features around Southern Africa, GLORYS was found to provide the best representation of the Agulhas Current (Russo et al., 2022), of particular importance to this study.

GLORYS is generated using a global ocean configuration of the Nucleus for European Modelling of the Ocean (NEMO) model. The model has a horizontal resolution of 1/12° ($\sim$7.5 km), while the vertical dimension is discretised using 50 z-layers with increasing resolution toward the surface. Atmospheric input to the model is obtained from the ERA5 atmospheric reanalysis (Section 2.2.5). GLORYS uses a reduced-order Kalman Filter scheme, including observations from delayed-time along track sea level anomaly data from all altimetric satellites, satellite Sea Surface Temperature (SST), Centre ERS d'Archivage et de Traitement (CERSAT) Sea Ice Concentration as well as in-situ temperature and salinity profiles from the Coriolis Ocean database ReAnalysis (CORA). The data are provided as daily mean values for the period 1993 to 2019, and are freely available from the Copernicus Marine Service (CMEMS) website[1].

2.2.2. CROCO regional simulation

While the GLORYS reanalysis product may currently be the preferred global product for the region of interest, it is hampered by a relatively coarse resolution ($\sim$7.5 km) which is insufficient to properly resolve sub-mesoscale features. This could be important in the context of this study, as sub-mesoscale eddies are known to develop in the inshore front of the Agulhas Current (Krug et al., 2017), which would serve to entrain oil onto the continental shelf. This study therefore considers output from a higher resolution ocean model configuration for the region (Tedesco et al., 2019), kindly made available by the South African Environmental Observation Network (SAEON).

The model output was generated using the Coastal and Regional Ocean COmmunity model (CROCO) (Debreu et al., 2012), which is built upon the Regional Ocean Modeling System (ROMS) (Shchepetkin and McWilliams, 2005). The CROCO configuration is comprised of a series of nested grids of increasing resolution over the area of interest. Figure 2.1 presents the spatial extent of the girds, showing how the size of the horizontal grid cells decreases from $\sim$22 km down to $\sim$0.75 km along the south eastern coast of South Africa. For this study, we

[1] http://marine.copernicus.eu/

consider only the ∼7.5 km (being at a comparable resolution to GLORYS) and ∼2.5 km domains, allowing us to consider the effects of enhanced model resolution on the trajectory and fate of oil. The vertical grid is comprised of 60 sigma (terrain following) levels, leading to particularly high vertical resolution in shallower waters on the continental shelf. A further advantage of the CROCO model output is that the vertical velocities and vertical eddy diffusivity variables are archived with the model output, while these variables are not typically archived with the global reanalysis products. An accurate representation of the vertical transport mechanisms can be important for the ultimate horizontal transport of oil (Röhrs et al., 2018). The model output data are available as daily mean values covering the period from 2000 to 2014.

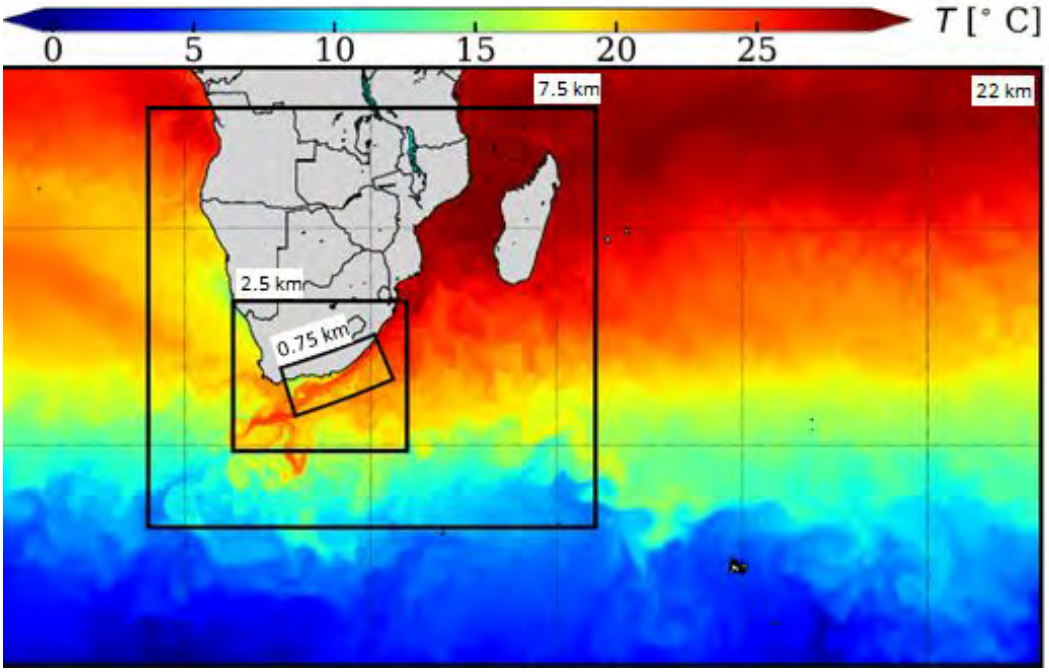

Figure 2.1: Geographic extent of the various domains of the CROCO regional simulation considered in this study (figure adapted from Tedesco et al., 2019). The colour denotes sea surface temperature at a snapshot in time from the model.

2.2.3. ACT array

Between April 2010 and February 2013, the Agulhas Current Time-series (ACT) mooring array measured the spatio-temporal variability of the Agulhas Current (Beal et al., 2015). The mooring array consisted of seven current meter moorings and four Current and Pressure recording Inverted Echo Sounders (shown in Figure 2.2), providing 12-hourly gridded cross sectional velocity data over the 250 km long array. The data represent the best available resource

for assessing the extent to which the Agulhas Current is represented in the available ocean models.

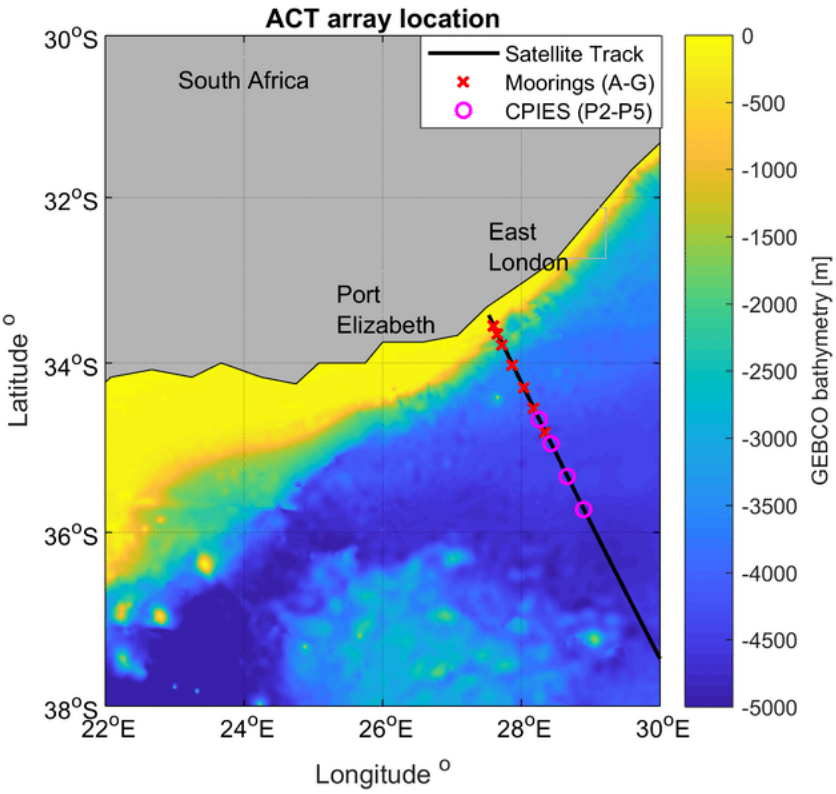

Figure 2.2: Geographical location of the ACT array with the moorings shown as red crosses and the CPIES (echo sounders) as magenta circles (Figure provided by Vermeulen et al. (2019)).

2.2.4. Satellite altimetry

Satellite observations of sea surface height provide useful data for validating model currents over a larger area than local in-situ observations, although the data are limited to the ocean surface and are low resoluton, typically ∼25 km. Here, we make use of daily delayed-time altimetry produced and distributed by CMEMS[2] spanning the period from 1993 to the present (Pujol and Mertz, 2019). The sea level anomaly data are used to compute geostrophic surface currents for comparison with model output.

[2]http://marine.copernicus.eu/

2.2.5. ERA5

Wind data for the oil spill modelling were obtained from the ERA5 atmospheric reanalysis product, available from the European Centre for Medium-Range Weather Forecasts (ECMWF)[3]. The horizontal wind vector components at 10 m above the surface are provided at hourly timesteps and at a spatial resolution of $\sim$25 km. The atmospheric input can be at a coarser spatial resolution than the ocean input because the spatial scales of atmospheric features are larger than those of the ocean (Pryor et al., 2012). The higher temporal resolution of the atmospheric input, however, allows for modelling sub-daily variability in wind-driven advection, for example due to land-sea breeze effects.

2.3. Ocean currents

Ocean current variability off the eastern and southern coastlines of South Africa is dominated by the Agulhas Current, one of the world's largest western boundary currents (Bryden et al., 2005). Here, we present model- and observation-derived data which highlight the important features of this current, while validating the model output against the observations. These data include surface geostrophic currents, eddy kinetic energy (EKE) and mean velocity and transport through the ACT array.

2.3.1. Surface currents

Figure 2.3 presents the mean surface geostrophic current speeds overlaid with the mean geostrophic current components, as derived from satellite observations and the three considered ocean model outputs, for the 14 year period covering the CROCO model output (Section 2.2.2). Geostrophic velocity components (u_g, v_g) are calculated based on gradients in sea surface height (η) as follows:

$$u_g = -\frac{g}{f}\frac{\partial \eta}{\partial y}, \qquad v_g = \frac{g}{f}\frac{\partial \eta}{\partial x} \tag{2.1}$$

where g is gravitational acceleration and f is the coriolis parameter:

$$f = 2\,\Omega\,\sin(\theta) \tag{2.2}$$

[3] https://www.ecmwf.int/en/forecasts/datasets/reanalysis-datasets/era5

where Ω is the earth's rotation rate and θ is the latitude. As the satellite data are provided at a lower resolution than the model outputs, all sea surface heights from the model outputs were interpolated onto the satellite data grid before computing the surface geostrophic velocity components.

Figure 2.4 presents the Eddy Kinetic Energy (EKE) derived from the geostrophic velocities computed from the satellite data and the model outputs. EKE is a diagnostic commonly used to depict the variability of ocean currents, and is computed as:

$$EKE = \frac{(u')^2 + (v')^2}{2} \tag{2.3}$$

where $u' = u_g - \bar{u_g}$ and $v' = v_g - \bar{v_g}$, where $\bar{u_g}$ and $\bar{v_g}$ are the mean surface geostrophic velocity components, calculated over the considered 14 year time frame.

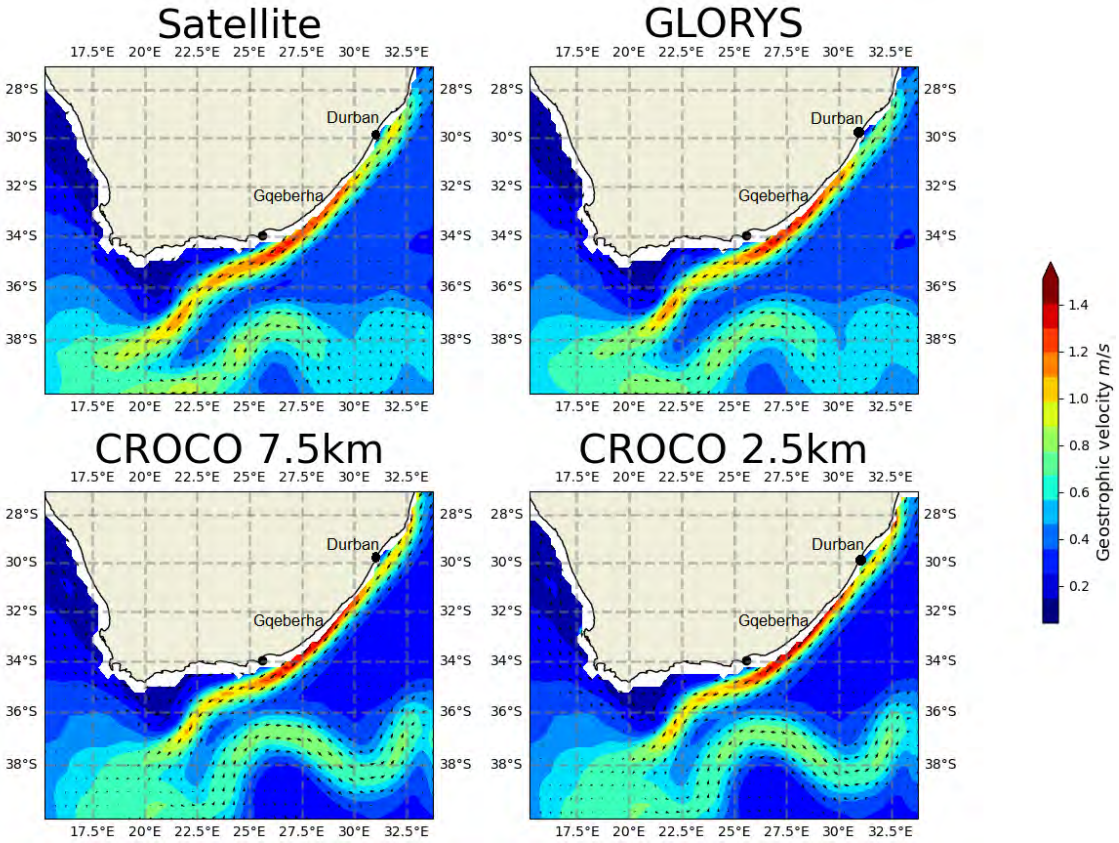

Figure 2.3: Mean surface geostrophic current speed overlaid with mean surface geostrophic current vectors, computed from sea surface height data from satellite altimetry, GLORYS and the two considered CROCO domains.

In agreement with the literature (Lutjeharms, 2006), the Agulhas Current is shown to originate off the coastline of the north-eastern extent of South Africa (~32°E), and flows along the

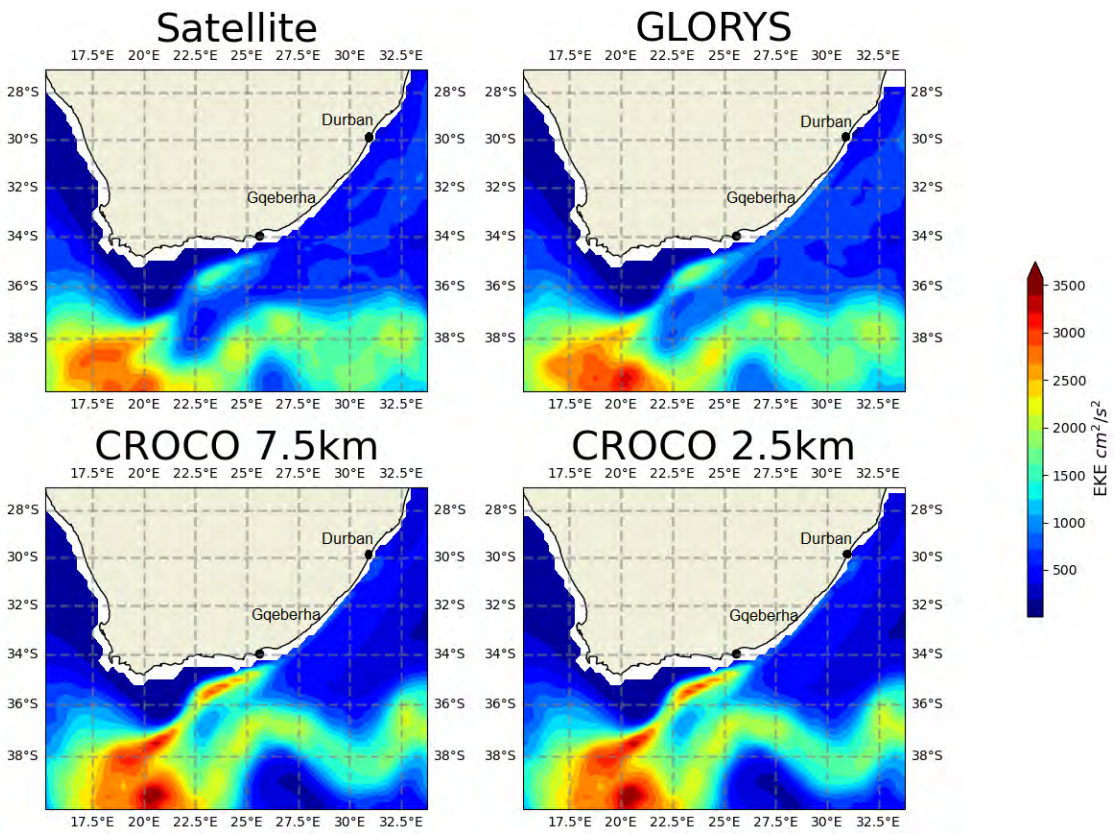

Figure 2.4: Eddy Kinetic Energy (EKE) computed from sea surface height data from satellite altimetry, GLORYS and the two considered CROCO domains.

east coast of South Africa before separating with the coastline south of Gqeberha (formerly Port Elizabeth), located on the eastern extent of the Agulhas Bank (Figure 2.3). The Agulhas Current typically retroflects between 19 and 20°E, before becoming the Agulhas Return Current which meanders back into the south-west Indian Ocean at a latitude of ∼38°S.

Figure 2.3 indicates that the highest current speeds are found along the coast between Durban and Gqeberha, where the mean surface geostrophic current speeds are in excess of 1.2 m s^{-1}. This region is however associated with low variability, as indicated by low EKE (Figure 2.4). South of Gqeberha, the current becomes less intense, however here we find higher variability (i.e. higher EKE) along the continental shelf, and particularly in the region of the retroflection. The Agulhas Current is therefore often described as being spatially ”bimodal” (e.g. Lutjeharms, 2006) in that the region upstream of Gqeberha is relatively fast flowing and stable, while downstream of Gqeberha it becomes less intense but more unstable. This instability is of particular importance for the transport of particles in the current, given that it can lead to more potential pathways of transport through meanders and eddies. In the context

of this study, eddies which occur along the inshore edge of the Agulhas Current (Krug et al., 2017; Tedesco et al., 2019) may drive the entrainment and retention of oil onto the continental shelf where they may be available for shoreline impacts.

The three considered model outputs are all shown to provide a reasonable representation the mean state of the system at the surface. Both considered CROCO domains do however tend to over-estimate EKE off the south coast and in the region of retroflection, while GLORYS typically shows better agreement with the satellite data. The differences are however considered to be small and the overall behaviour is well represented in all models. This is particularly encouraging since the CROCO configuration does not include data assimilation, unlike GLORYS which does.

2.3.2. Variability through the ACT array

While the satellite altimetry data are useful for providing a description of the surface ocean currents, in-situ data from the ACT array are particularly useful for providing insight into the vertical structure of the Agulhas Current. Figure 2.5 presents a comparison of mean alongshore velocity between the ACT array, GLORYS and the two considered CROCO domains, all computed over the time period for which data from the ACT array are available. Volume transport, or the volume of water travelling through the ACT array, can be a useful diagnostic for summarising the state of the Agulhas Current. Figure 2.6 presents histograms of volume transport through the ACT array, indicating the range of transports over the observation period. We note that only the upper 2000 m of the water column are considered in the transport analysis to focus on the variability in the core of the current, with less emphasis on the effects of the under-current.

In agreement with the presented surface geostrophic currents, Figure 2.5 shows near-surface mean current velocities in excess of 1 m s^{-1} in the main core of the current, and that these velocities extend $\sim$100 km offshore and to a depth of $\sim$200 m, close to the sea floor. Also evident is a weaker undercurrent which typically exists at depths greater than 2000 m in the mean state. The models are all shown to perform well when compared with the in-situ data, both in depth and in horizontal extent. The higher resolution of the 2.5 km CROCO domain is however evident in that the representation of the current is less pixelated. Figure 2.6 indicates that the observed southward transports are generally higher in the observations than in the

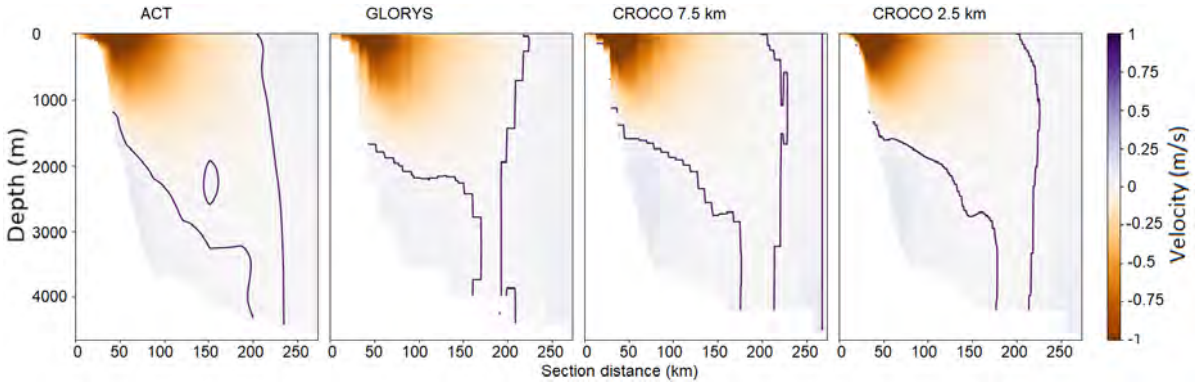

Figure 2.5: Comparison between in-situ data and model output at the ACT array, indicating mean alongshore velocity through the section of the array. The shown contour indicates zero velocity.

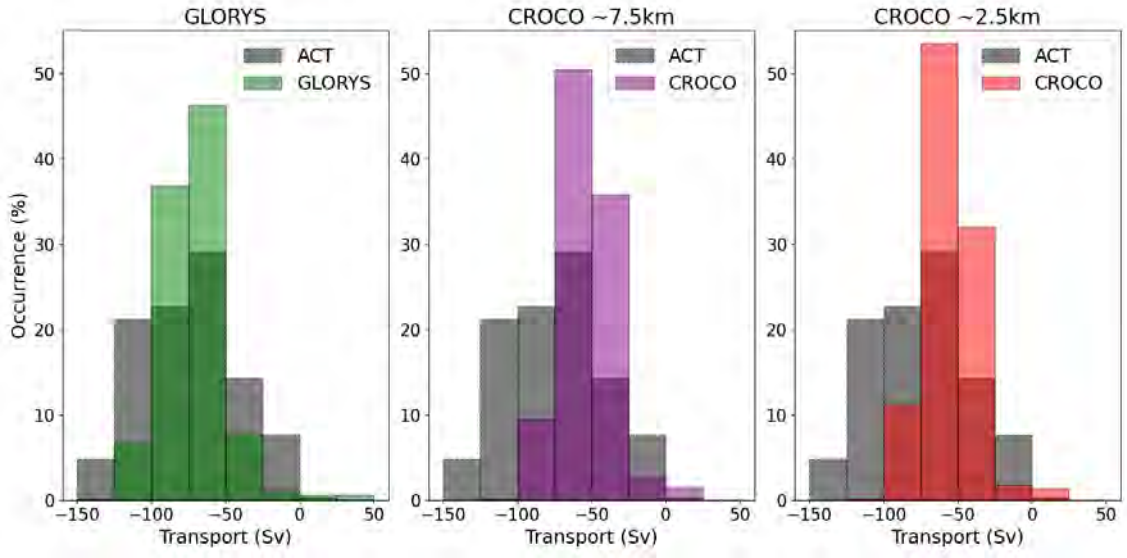

Figure 2.6: Histogram comparisons of in-situ and model daily transport through the ACT array. The analysis is restricted to the upper 2000 m of the water column. Transports are plotted in units of Sverdrup (1 Sv = 10^6 m^3 s^{-1})

models (more negative transport implies greater southward transport) and cover a wider range (as indicated by a flatter histogram).

Notwithstanding the identified model discrepancies, all three models are considered to represent suitable oceanographic input to the oil spill model. The GLORYS product provides the closest fit to the observations in the mean state, which is not surprising given that GLORYS is assimilated with observations, while the CROCO simulation is not. In this study we however opt to use the CROCO model output as the preferred input to the oil spill model, given that it allows us to test the effect of model horizontal resolution on the fate of oil, and the output includes vertical velocities and vertical eddy diffusivity variables which are not routinely available with GLORYS.

2.3.3. Variability at the east coast well location

Here, we present ocean current data at the modelled east coast well location (30.5396°S 31.7799°E, as described in Section 3.1), providing a detailed account of the current variability in the vicinity of the modelled blowout. Figure 2.7 presents current roses at the surface and at a depth of 2800 m (near the seabed), while daily mean and daily maximum current speeds throughout the year at these depths are presented in Figure 2.8. Note that current direction is by convention the direction toward which the current is flowing, as apposed to wind direction which is from where the wind comes.

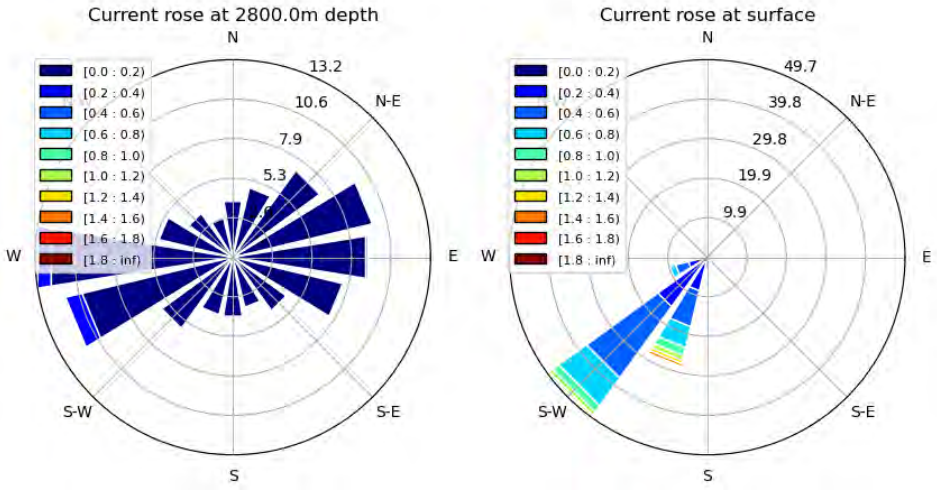

Figure 2.7: Current roses at the surface and at 2800 m depth at the modelled east coast well location based on 14 years of the 2.5 km resolution CROCO model output (units are m s^{-1}).

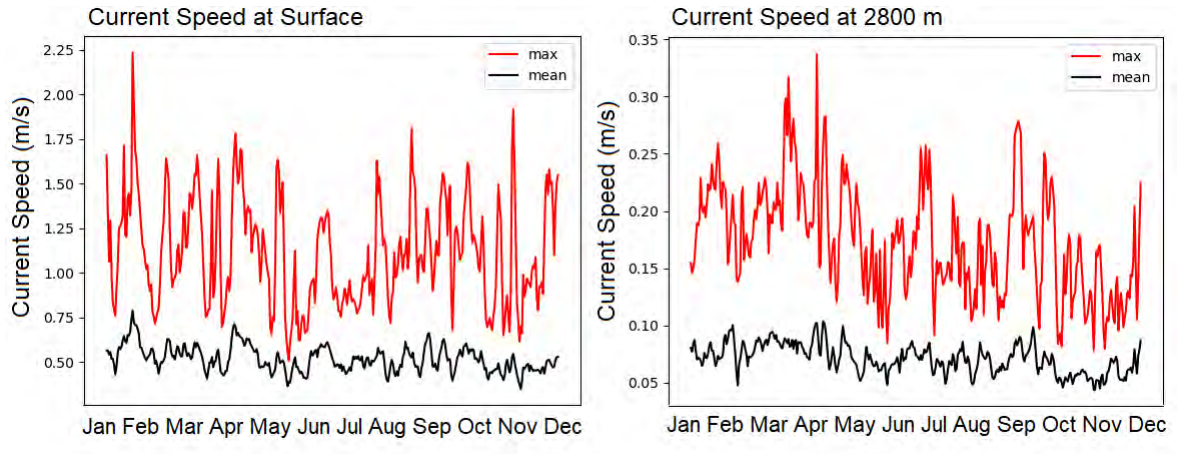

Figure 2.8: Daily mean and daily maximum current speeds at the surface and at 2800 m depth at the modelled east coast well location based on 14 years of the 2.5 km resolution CROCO model output.

The current rose for the surface shows the low degree of variability in current direction,

with SW to SSW representing the dominant direction. The current rose at 2800 m depth shows a much larger range of directions, although the current speeds are considerably lower. Figure 2.8 shows maximum surface speeds in excess of 2.25 m s^{-1} while the near-bottom indicates a maximum speed slightly below 0.35 m s^{-1}. The mean speeds are 0.6 m s^{-1} and 0.075 m s^{-1} for surface and near-bottom currents, respectively. Figure 2.8 indicates no clear seasonal variation in currents at this location near the surface or at depth.

2.4. Surface winds

Given the range of latitudes, surface winds over the study area are under the influence of both tropical and mid-latitude dynamics. Here, we present model-derived data which highlights the important large scale features of surface winds over the study area, with an emphasis on the seasonal variability in winds, as this tends to be higher than that of the large scale current features in the region.

2.4.1. Spatial variability

Figure 2.9 presents seasonal mean wind speeds overlaid with mean wind vectors, computed from ERA5 (Section 2.2.5). For the purposes of this analysis, nominally summer and winter periods are taken as the six month periods of October to March and April to September, respectively.

The seasonal variability in the winds over the region are largely dictated by the migration of the South Atlantic and South Indian Ocean high pressure cells, associated with anticyclonic (anticlockwise in the southern hemisphere) circulation around each (Preston-Whyte, 1988). Strong westerly winds in the southern extent of the shown domain are associated with the passage of mid-latitude pressure systems, which shift northward during winter, in accordance with the northward migration of the South Atlantic and South Indian Ocean high pressure cells. Winds off the west coast of Southern Africa are, in the mean state, shore parallel and equatorward all year round, but are stronger in summer. Off the south and east coasts, winds in summer are shown to be weaker on average, and associated with a stronger easterly component. It should be noted that regions where the mean wind vector is close to zero (e.g. off the east coast in winter), implies that there is no dominant direction in the mean wind vectors.

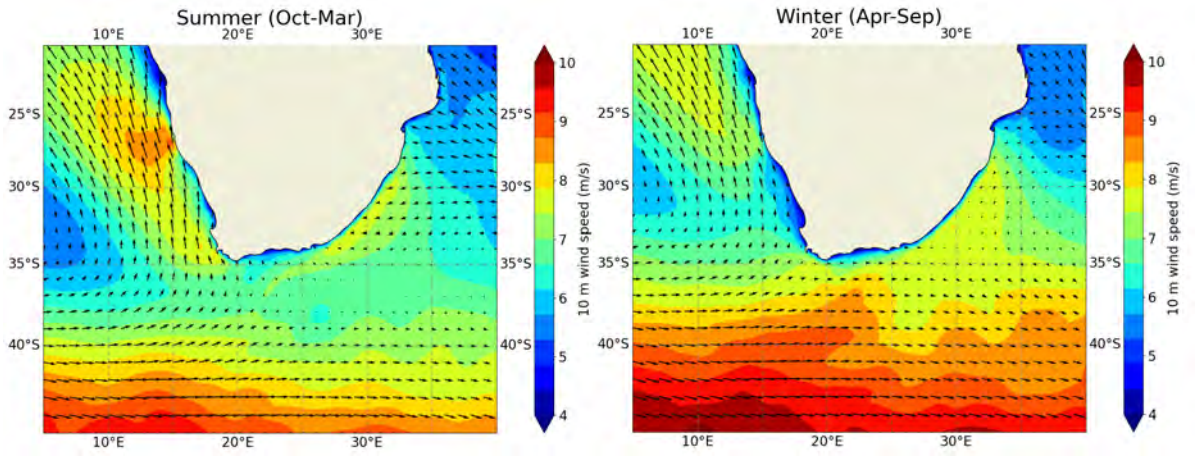

Figure 2.9: Seasonal mean 10 m wind speed overlaid with mean 10 m wind vectors, computed from 14 years of data from ERA5.

2.4.2. Variability at the east coast well location

Figure 2.10 presents seasonal wind roses at the modelled east coast well location (30.5396°S 31.7799°E, as described in Section 3.1), while daily mean and daily maximum surface wind speeds throughout the year are provided in Figure 2.11. Note that the wind direction is by convention the direction from which the wind is blowing.

The seasonality in the wind speeds at the modelled east coast well location is evident in Figure 2.11, which indicates a maximum mean wind speeds around September and a minimum in March. Wind direction is generally shown to be orientated along the NNE-SSW axis at this location. The strongest winds occur in winter from the SSW, while summer is associated with a greater easterly component, in agreement with Figure 2.9.

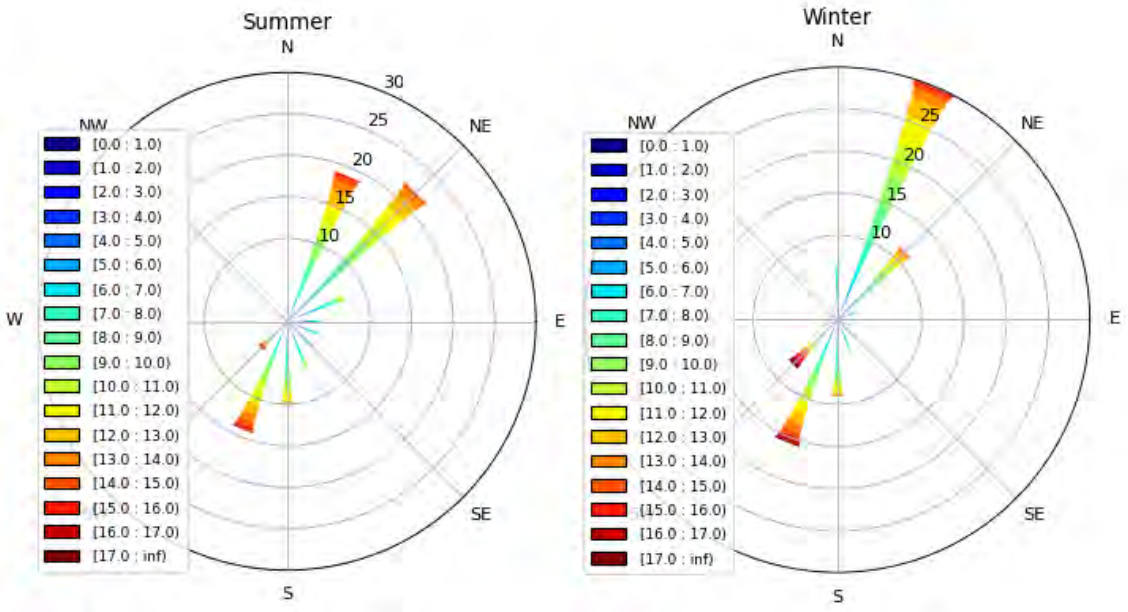

Figure 2.10: Seasonal wind roses at the modelled east coast well location based on 14 years of data from ERA5 (units are m s^{-1}).

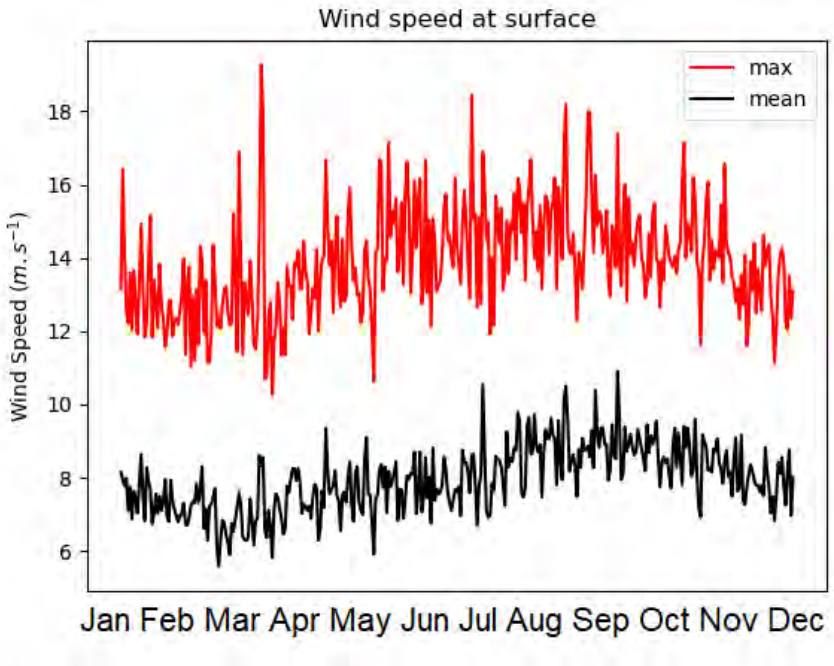

Figure 2.11: Daily mean and daily maximum surface wind speeds at the modelled east coast well location based on 14 years of data from ERA5.

3

Methods

3.1. Blowout spill scenarios

There are a number of potential spills which could occur during oil exploration drilling, including surface spills of marine diesel, accidental releases of Non Aqueous Drilling Fluid (NADF), and blowout spills at the wellhead on the seafloor. Blowout spills pose the greatest potential environmental impact and are therefore the focus of this study.

For the purposes of modelling, blowout spill scenarios need to be defined according to the spill location, the properties of the oil released (e.g. density, viscosity, gas-to-oil ratio, droplet size distribution etc.), the flow rate from the well on the seabed and the release duration. The details of the spill scenarios to be modelled are associated with large uncertainty, particularly when exploratory wells have not yet been drilled and the details of the oil prospect are still largely unknown. In this study we rely on the information provided in the oil spill modelling study undertaken by ERM which deals with potential spills from Block ER236 off the east coast of South Africa (ERM, 2018).

ERM (2018) considered blowout scenarios from two locations within Block ER236 - a deeper location in $\sim$2900 m water depth and a shallower location in $\sim$1600 m water depth. The adopted flow rates for these locations were 1 050 m^3d^{-1} (6 604 bpd) and 750 m^3d^{-1} (4 717 bpd) for the deeper and shallower locations, respectively. By way of context, estimates of the flow rate from the Macondo / Deepwater Horizon blowout spill are often cited in the range of 50 000 to 70 000 bpd. The ERM (2018) flow rates are therefore an order of magnitude less than the DWH spill, however it is acknowledged that expected flow rates are extremely site specific. The expected flow rate would in reality depend on the characteristics of the reser-

voir – pressure, temperature, formation characteristics, depth below surface and the drilling technology employed. Here, we take the ERM (2018) flow rates at face value and use these unchanged in our model. Although we modelled potential spills at both the deeper and shallower east coast sites we only present results for the deeper well as the flow rate is higher and therefore more conservative with respect to potential ecological impacts.

ERM (2018) considered spill durations of 7 and 20 days. The 7 day scenario corresponded to the blowout ending due to the hole collapsing upon itself, while the 20 day scenario corresponded to the scenario where the the blowout was capped using a capping stack. The Oil Spill response Limited (OSRL) Consortium does indeed hold a subsea capping stack in Saldanha Bay, located on the west coast of South Africa. The capping stack would however take no less than a week to be transported to the spill location (dependent on sea conditions). Deployment of the equipment over the ruptured riser pipe would be complicated by the extreme oceanographic environment in the form of intense currents (Section 2.3) and high waves. The strong currents oppose the predominant swell direction, which amplifies wave heights with the Agulhas Current and promotes the formation of freak wave events (Ponce de León and Guedes Soares, 2021; Lavrenov, 1998). In this study we consider a 15 day blowout duration to correspond to the best case scenario of either a hole collapse or the rapid deployment of a capping stack. It is considered prudent to also consider a 60 day scenario, in the event that the hole does not collapse naturally and/ or complications with the installation of the capping stack. Again, as a point of reference, the Macondo/ Deepwater Horizon blowout spill lasted 87 days. For both spill durations we run the model for a total of 90 days, to track the ultimate fate and transport of the spilled oil in the environment after the spill has ended.

Although there remains uncertainty as to the characteristics of the prospect, the hydrocarbon in this region is expected to be oil (as opposed to gas), and the oil viscosity is expected to be light (ERM, 2018). Details of the light crude oil adopted in the modelling in this study are further explored in Section 3.3.3.

While the focus of this study is on Block ER236 off the east coast of South Africa, we also test the sensitivity to modelling the same hypothetical spill (oil type, flow rate and flow duration) from two other locations where light crude oil is also being targeted off the coast of South Africa; namely from south coast and west coast locations. The considered south coast spill location is in the southern extent of Block 5/6/7 (19.225°E, 35.879°S), while the considered

west coast spill location is within the Deep Water Orange Basin Block (14.25°E, 30.5°S). We note that there is planned exploration and production drilling planned in Block 11B/12B, located off the continental shelf between Mossel Bay and Gqeberha, although the prospect there is expected to be gas condensate, and so the oil characteristics modelled herein are considered less applicable.

It is acknowledged that the different modelled well site locations will have differences in the expected flow rates and oil characteristics, however we maintain the same spill scenario for each location. This is considered useful in that it isolates the effect of the varying oceanographic and atmospheric features on the trajectory of a hypothetical oil spill from different locations around the coastline, and is therefore presented as a sensitivity test.

3.2. Model description

In this study we make use of the OpenOil module of OpenDrift[1] (Dagestad et al., 2018), an open-source software package designed for modelling the trajectories and fate of objects or substances drifting in the ocean. The substance being simulated is treated as an assemblage of particles whereby each particle is representative of a fraction of the total mass of the substance. Particles are transported both horizontally and vertically in the model in a variety of ways, as briefly described below.

Subsurface particles are transported by the prevailing ocean currents, while horizontal and vertical diffusion (due to unresolved turbulence) are modelled as random walk processes. Subsurface particles are also transported vertically due to the difference in density between the substance and the ocean - oil is less dense than seawater and is therefore positively buoyant. The terminal vertical rise velocity depends on the Reynolds number for the flow around the oil droplet, following the Stokes law for low Reynolds numbers and an empirical expression for higher Reynolds numbers (Tkalich and Chan, 2002). Once on the surface of the ocean, particles can be additionally transported by surface winds and stokes drift (due to surface gravity waves), although advection due to stokes drift is not implemented in this study. Surface particles can once again be entrained into the subsurface through wave entrainment (often referred to as 'dispersion'), which is a function of the wind-driven sea state (surface gravity waves) and oil properties. Modelling wave entrainment in this way results in a continuous

[1] https://github.com/OpenDrift/opendrift/

exchange between the surface and entrained oil such that the submerged oil acts as a reservoir that constantly releases oil to the surface, which is in turn entrained by subsequent wind/wave events. Details of the implementation of wave entrainment in OpenOil are provided in Röhrs et al. (2018).

Oil weathering is included in the model via the Automated Data Inquiring for Oil Spills (ADIOS) weathering module that is available as an open-source package from the US National Oceanic and Atmospheric Administration (NOAA)[2]. The ADIOS model includes an oil database of more than 1000 crude and refined oil types, and includes weathering processes of evaporation, dispersion, spreading and emulsification, i.e. that are most relevant on timescales of hours to days. As described above, dispersion is however not treated as a weathering process in OpenOil as wave entrainment is handled explicitly in the vertical mixing scheme.

We note that the ADIOS model excludes the longer-term weathering processes such as biodegradation, photo-oxidation and sedimentation, which would result in the model tending to overestimate the amount of oil remaining on the surface for periods longer than a week after the spill. There is however considerable uncertainty regarding the site- and oil-specific weathering rates for these longer-term processes. The level of sophistication in the oil weathering parameterisation should also be viewed in light of the large uncertainty associated with the oil spill scenarios being modelled.

3.3. Model configuration

3.3.1. Representation of the near-field

Deepwater blowouts are characterised by a large flow of a mixture of oil and gas at high pressure through a relatively small orifice (or multiple orifices), leading to large vertical velocities and high turbulence in the vicinity of the well head. In the region of tens to hundreds of metres from the well head, termed the ”nearfield”, plume dynamics are dominated by the turbulence associated with the buoyant jet. Once sufficient seawater has been entrained, the plume reaches a “trap height”, after which the transport of oil becomes dominated by the advection and mixing associated with the prevailing ocean currents. Gas bubbles and and oil droplets which coalesce within the nearfield then rise to the surface at their own terminal velocities

[2]https://github. com/NOAA-ORR-ERD/OilLibrary

which are a function of their density and gas/droplet size distributions.

The farfield modelling of oil transport, being the focus of this study, requires estimates of the trap height, the horizontal extent of the nearfield plume, and the oil droplet size distribution resulting from the nearfield processes. Here, we seed the model with particles at a trap height of 100 m off the seabed, and a horizontal radius of 100 m. These values were selected based on near-field simulations using the Texas A&M Oilspill Calculator (TAMOC) model[3], although it is noted that the far-field model results are not particularly sensitive to these inputs, given their spatial scale relative to the depth of the release and the large horizontal distances oil is transported in the far-field model. The modelled droplet size distribution does however play a key role in the far field model, as described in Section 3.3.2 below.

3.3.2. Oil droplet size distribution

Knowledge of the oil droplet size distribution (DSD) is one of the most important factors which determine the farfield trajectory and fate of oil from deepwater blowout events (Zhao et al., 2017). Larger droplets rise quickly to the surface, while smaller droplets can be transported great distances by ocean currents before surfacing, particularly in high energy current regimes such as considered in this study. The oil droplet size distribution is ultimately determined by the physical-chemical properties of the release (e.g. gas to oil ratio, viscosity, density, oil-water interfacial tension) and the turbulence of the flow field (Li et al., 2017b). Smaller droplets can be formed by increasing turbulence (e.g. by reducing the orifice diameter) or by decreasing the interfacial tension (e.g. by applying chemical dispersants at the release).

Both the lognormal and Rosin-Rammler distribution functions have shown to provide a reasonable approximation to empirical data on DSD's for oil from subsea blowouts (Johansen et al., 2013), although there is no theoretical basis for choosing a particular distribution function (Chen and Yapa, 2007). For the purposes of this study, we adopt a lognormal distribution for initialising droplet diameters, which implies that the logarithms of the droplet sizes follow a normal distribution. The lognormal distribution can be generated if one has knowledge of the mean or median (d_{50}) diameter and the standard deviation (σ) of the distribution. There is however large uncertainty around the selection of d_{50} and σ for input to the model. Even in the case of the Deepwater Horizon spill, for which there are a number of observations, there re-

[3] https://github.com/socolofs/tamoc

mains ongoing debate as to true DSD resulting from the blowout. Things were complicated in the case of the Deepwater Horizon spill, as oil escaped from multiple orifices of varying diameter (kink holes and the riser outlet) and that the application of dispersants was not constant in time (Spaulding et al., 2017; French-McCay et al., 2021a). French-McCay et al. (2021b) suggest that the DSD from the Deepwater Horizon Spill was bimodal, with 74% of the oil mass in >1 mm droplets that surfaced near the spill site within a few hours, and 1 – 8% as <0.13 mm microdroplets that remained below 900 m. Future large blowout spills are likely to face similar circumstances, making the selection of a DSD for input to the model a difficult task. Field data, experimental data and nearfield models all generally indicate that an untreated blow-out (i.e. without application of dispersants) results in oil droplet diameters with a d_{50} in the order of millimeters, while the application of dispersants can reduce this by an order of magnitude (Brandvik et al., 2021; Johansen et al., 2013; Spaulding et al., 2017; Zhao et al., 2017).

Here, we take the pragmatic approach of modelling two DSD's which cover a reasonable range of DSD's typically found in the literature (Figure 3.1). DSD 1 corresponds to the scenario of no to low application of dispersants which result in faster riser droplets, while DSD 2 corresponds to the scenario where dispersants are applied and/or the release is from a particularly small orifice (e.g. a kink in the riser pipe).

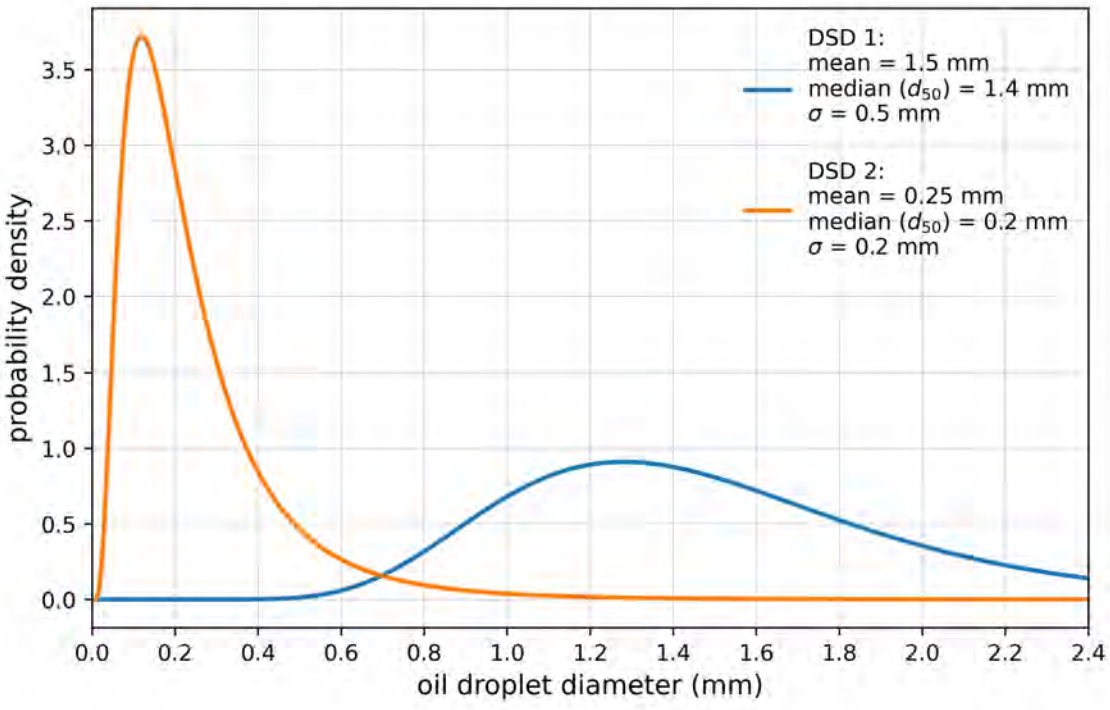

Figure 3.1: Modelled oil droplet size distributions.

Figure 3.2 provides the rise velocity as a function of oil droplet diameter for the oil type considered in this study, as implemented in OpenOil. The figure indicates that droplets with a diameter of 1.4 mm (d_{50} for DSD 1) would take less than a day to reach the surface from a release depth of 2 700 m (the approximate depth at which particles are initialised in the model), while droplets with a diameter of 0.2 mm (d_{50} for DSD 2) would take about 19 days to rise the same distance.

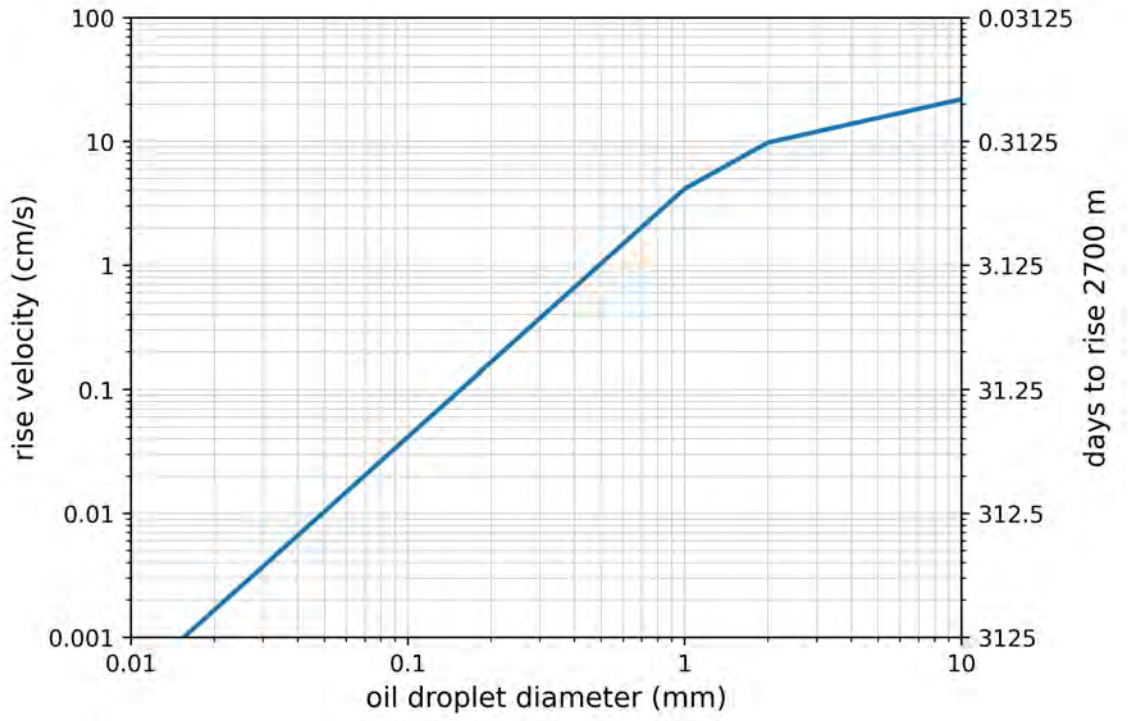

Figure 3.2: Rise velocity as a function of oil droplet diameter for the Norman Wells light crude oil (density = 837.5 kg m-3) in seawater (temperature = 15 °C, salinity = 35 psu). Also shown is the number of days it would take for an oil droplet to rise 2 700 m (the approximate release depth in the model) at the shown rise velocities.

As described in Section 3.2, droplets which reach the surface can be entrained once again by wind-driven waves. This turbulence generates a new droplet size distribution for the particles which have become entrained. Following Röhrs et al. (2018), we adopt the estimation of the droplet size distribution and wave entrainment rate according to Li et al. (2017b) and Li et al. (2017a), respectively.

3.3.3. Oil properties and weathering

As mentioned in Section 3.1, there remains large uncertainty around the chemical properties of the crude oil to be targeted during exploration drilling in Block ER 236, however the ENI

oil and gas company is expecting the oil viscosity to be light. For the purposes of modelling in this study, we adopt the 'Norman Wells' oil from the ADIOS oil database[4], which we take as a generic light oil for which sufficient data are available for modelling. Figure 3.3 presents the sensitivity of the mass balance and oil properties for a surface release of Norman Wells under a range of constant wind speeds. It should be noted that the application of a constant wind speed is highly unrealistic, but is presented purely as a sensitivity test on the ADIOS weathering algorithms as implemented in OpenDrift.

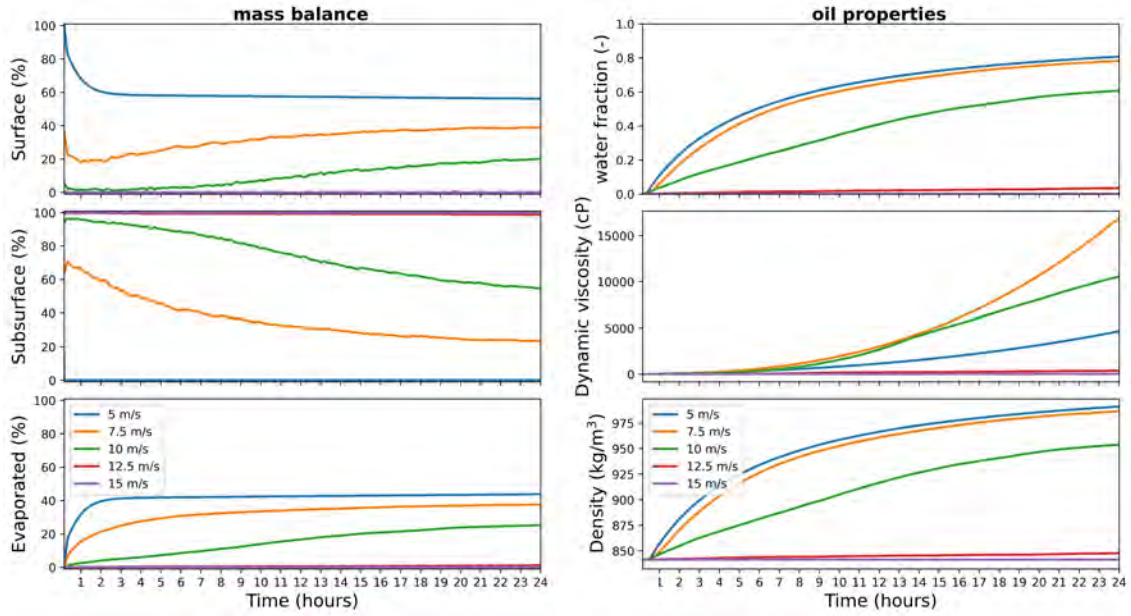

Figure 3.3: Sensitivity tests on the ADIOS weathering algorithm for a surface release of the 'Norman Wells' light crude oil under a range of constant wind speeds.

For a low wind speed of 5 m s^{-1}, no oil is entrained into the subsurface and about 40% of the mass of oil evaporates within a few hours. This rapid evaporation is accompanied by the onset of emulsification, which increases the water fraction in oil to around 80% within the first day. The density of the emulsion thus gradually approaches that of water, while the viscosity increases by several orders of magnitude. For higher wind speeds of 12.5 m s^{-1} or greater, the turbulence at the water surface does not permit the presence of surface oil and almost all of the oil is maintained in the subsurface, thereby preventing evaporation or emulsification.

[4]https://adios.orr.noaa.gov/oils/EC00654

3.3.4. Shoreline interaction

A high resolution land mask taken from the GSHHG database[5] is used in OpenOil to represent the boundary between the ocean and land. When particles make contact with land they become stranded and are deactivated from the simulation. This is a conservative approach with respect to land impacts as there is no limit to particles stranding in close proximity, while in reality different types of shorelines have different holding capacities which may tend to prohibit stranding of additional oil once saturated (Gundlach, 1987). Any particles which might make contact with the seabed are not deactivated but are simply lifted to the depth of the seabed.

3.3.5. Other numerical settings

Horizontal and vertical diffusivity are included in the model as random walk processes. A constant horizontal diffusivity of 5 m^2s^{-1} is adopted, while a spatial and temporal varying vertical diffusivity is obtained from the turbulence closure scheme implemented in the CROCO simulation providing the ocean current input.

For the wind drift factor (the fraction of the wind speed used in the advection of surface oil), we adopt the commonly accepted value of 3% of the wind speed (Wu, 1983).

The 15 day blowout scenario is simulated using 2 500 particles (lagrangian elements), approximately equating to a release of 7 particles every hour. Given a flow rate of 1 050 m^3d^{-1}, each particle represents 5 291 kg of oil upon initialisation (i.e. prior to weathering). The 60 day blowout scenario is simulated using 10 000 particles, thereby maintaining the same initial oil mass per particle as used in the 15 day blowout scenario.

A time-step of 1 hr is used for the advection of particles, while vertical mixing is simulated on a smaller time-step of 1 min. The oil properties (mass, density, viscosity, water content etc.) and coordinates (horizontal and vertical) of each particle are saved at 3 hourly time-steps over the duration of each simulation.

3.4. Stochastic modelling approach

The fate of a given oil spill is dependent on the prevailing currents and winds over the duration of the spill. As these parameters vary greatly over time, it is important to simulate the spill un-

[5] https://www.soest.hawaii.edu/pwessel/gshhg/

der many combinations of winds and currents in order to ascertain the probability of oiling at any given location of interest. To this end, each spill scenario is simulated 200 times. Each simulation, or iteration of the spill scenario, is kept identical in the model setup, differing only in the start time of the simulation. The start time of the simulations undertaken in this study cover the five-year period from 2007 to 2012 (implying 9.13 day increments between successive simulations). This is considered sufficiently long so that the average environmental conditions over the modelled period well approximate the underlying current and wind climatologies forcing the model.

By modelling each spill scenario 200 times, it is possible to use the ensemble of model outputs to determine the likelihood of a particular outcome. For example, one may be interested in the probability that a particular sensitive receptor will be impacted by surface or shoreline oiling over a given threshold defined in Table 3.1. This is achieved by simply summing the number simulations where the threshold of interest was exceeded at the sensitive receptor, and dividing by the total number of simulations. Carrying out this calculation on many locations over the model domain (on a regular grid, as discussed in Section 3.5.1), allows us to produce spatial maps which indicate the probability that a particular threshold would be exceeded.

3.5. Analysis of model output

3.5.1. Computation of concentrations from Lagrangian elements

The first step in the analysis of the model out is to compute concentrations of surface, stranded and subsurface oil from the raw model output. These concentrations are computed for every output time-step of every simulation. While the raw model output is comprised of oil properties at the locations of the particles (Lagrangian elements), the concentrations are computed on a regular Eulerian grid with a horizontal resolution of 7.5 km.

It is important to note that the oil mass used in mass budgets (e.g. Figure 3.3) does not take the total mass of the oil-water emulsion into account. This can be an important consideration in the case of surface and stranded oil, where it is desirable to estimate the volume of oil-water emulsion floating on the water surface or stranded on the shoreline. The mass of the oil-water emulsion is computed following the OpenOil documentation as follows:

$$mass\_emulsion = \frac{mass\_oil}{1 - water\_fraction} \tag{3.1}$$

The volume of the oil-water emulsion can then be computed using the density of the oil-water emulsion, which is a direct output from the model (e.g. Figure 3.3). The maximum water fraction implemented in the model is 0.9, implying that the mass of the oil-water emulsion can be as much as 10 times higher than the mass of the raw oil. Surface oil thickness is then computed as the sum of the volume of the surface oil-water emulsion within each 7.5 km x 7.5 km grid cell divided by the area of the grid cell.

The computation of shoreline oil concentration, in g m^{-2}, requires an estimation of a width of shoreline over which the shoreline oil is likely to be deposited. For this study we use a constant value of 30 m for this purpose, which can be thought of as the horizontal distance of the inter-tidal zone, considering a 1.5 m tidal range (the approximate average tidal range for South Africa) and a 1:20 shoreline slope.

Subsurface concentrations are computed on a regular vertical grid with a resolution of 50 m using the mass of oil (not the oil-water emulsion as described above). The computation cost of this calculation necessitated limiting the extent of subsurface concentrations, as will be shown in Section 4.1.

3.5.2. Consequence thresholds

It is important to compare the computed surface, stranded and subsurface oil concentrations against consequence thresholds, so that the model results can be related to potential real world impacts. Table 3.1 provides a summary of the consequence thresholds adopted in this study, and a brief description of the associated impacts, which have been taken from the literature (French et al., 1996; French-McCay, 2004).

Table 3.1: Consequence thresholds used in the analysis of the model output.

Threshold type	Threshold	Visual appearance	Associated impacts
Surface oil thickness	0.01 μm	Barely visible silver sheen	Onset of socio-economic impact, likely affecting fisheries, aquaculture, seawater intakes and recreational activities
	1 μm	Rainbow sheen	Smothering of seabirds and other wildlife
	10 μm	Deep brown or metallic sheen	Mortality of seabirds and other wildlife
Shoreline oil concentration	1 g m^{-2}	May appear as a coat, patches or scattered tar balls, stain	This level would trigger the need for shoreline cleanup
	100 g m^{-2}	May appear as black opaque oil	Shoreline life is significantly affected by this level of oiling including mortality of seabirds and other wildlife
Subsurface oil concentration	100 μg L^{-1}	N/A	Conservative screening threshold for potential effects on sensitive organisms. Soluble PAHs are approximately 1% of the total oil so threshold corresponds to 1 μg L^{-1} of dissolved PAHs

4

Results

4.1. 15 day blowout: examples of individual deterministic simulations

We begin by presenting results from two individual simulations, with the intention of providing insight into the raw model output, and the process of computing concentrations from these data. These are just two simulations from a total of 200 simulations carried out for the east coast 15 day blowout scenario; one to illustrate an example which significantly impacted the east coast of South Africa (Figures 4.1 and 4.2) and one which significantly impacted the south coast (Figures 4.3 and 4.4). The results for both modelled droplet size distributions (DSD 1 and DSD 2 as described in Section 3.3.2) are shown for comparative purposes.

Figure 4.1 presents snapshots of the modelled particle locations for an example simulation which resulted in significant oiling on the east coast of South Africa. For reference, this represents the 88th percentile simulation in terms of shoreline length oiled above the 1 g m^{-2} threshold for DSD 1. The results indicate how for DSD 1, oil is brought rapidly to the surface, where it is quickly advected down the east coast of South Africa, predominantly by the Agulhas Current. In the case of DSD 2, the pattern of surface oil is similar, although a large portion of the released oil is maintained at depth, as expected from the slower rise velocities of this DSD (Figure 3.2). Both simulations indicate significant interaction of oil with the east coast, as shown in the snapshots at 15 days after the start of the spill (Figure 4.1). The results at 30 days after the start of the spill indicate that some oil is entrained onto the Agulhas Bank off the south coast of South Africa, a large portion of oil reflects the Agulhas retroflection and return current (Figure 2.3), while some oil is maintained on the east coast between Durban

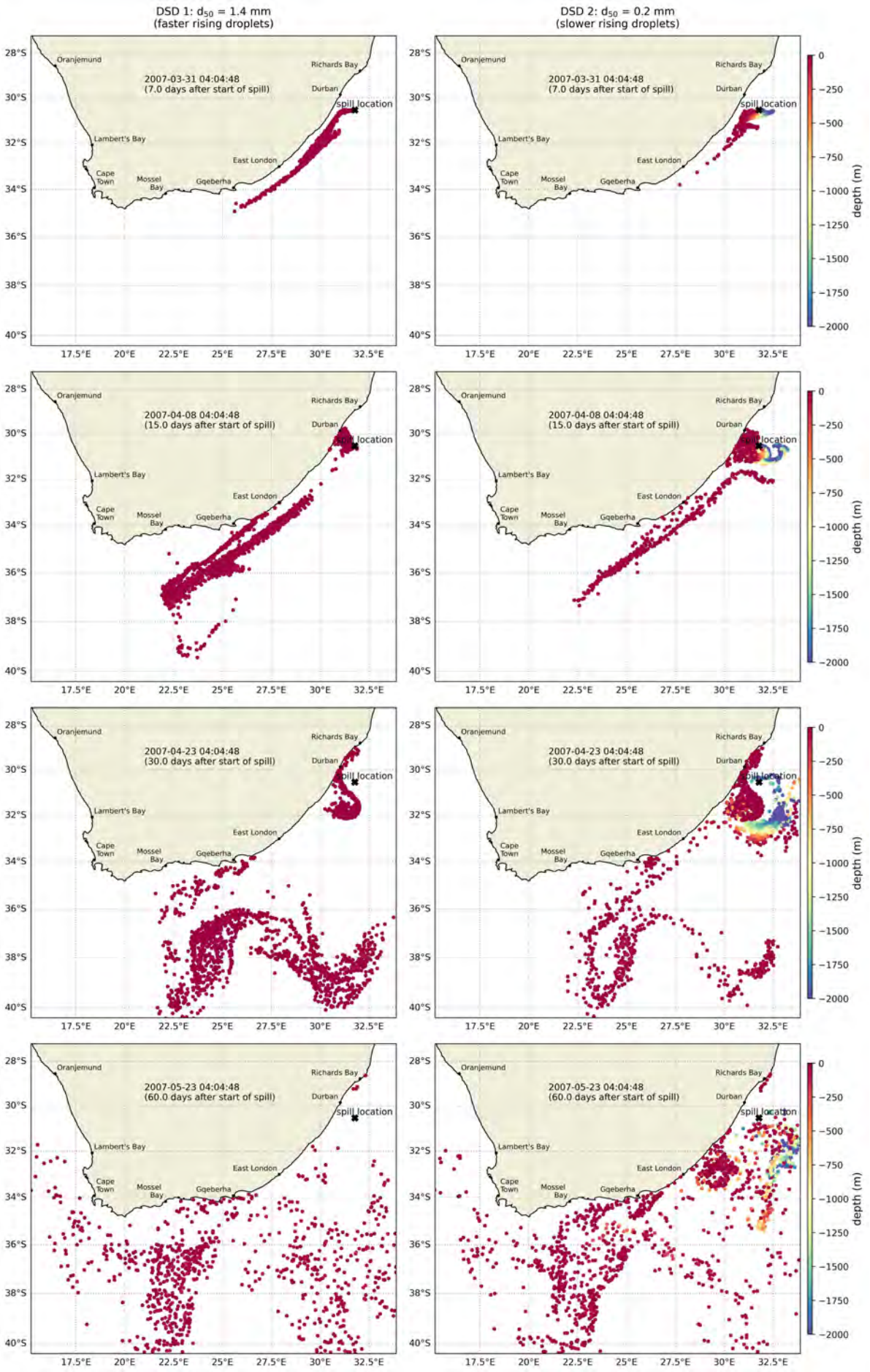

Figure 4.1: East coast 15 day blowout: modelled particle locations at snapshots in time for an example simulation which resulted in significant oiling on the east coast of South Africa.

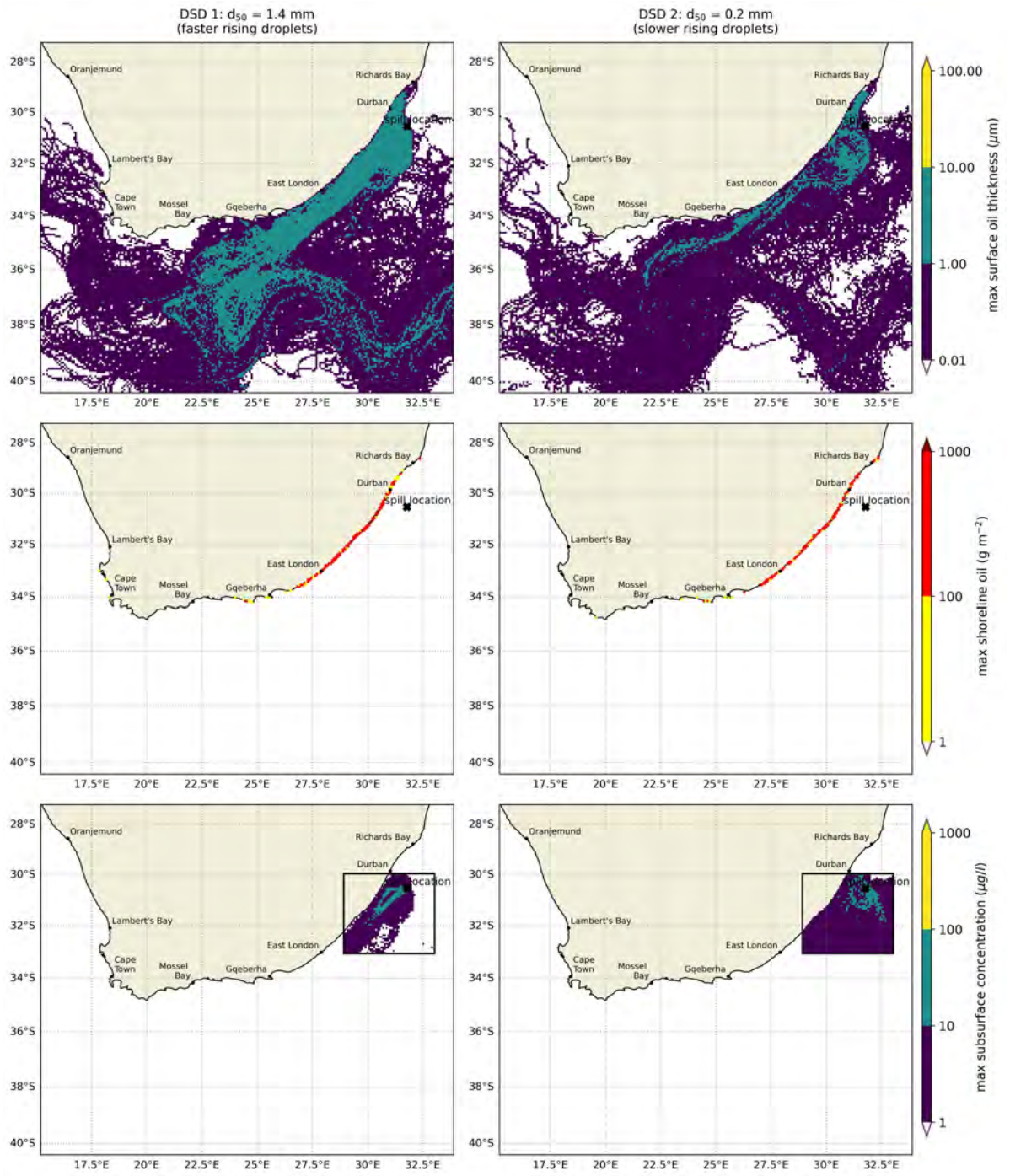

Figure 4.2: East coast 15 day blowout: modelled surface oil thickness (top panels), stranded oil concentration (middle panels) and subsurface oil concentration (bottom panels) for an example simulation which resulted in significant oiling on the east coast of South Africa. The values delineating different colours reflect the consequence thresholds presented in Table 3.1 e.g. the green in the top panels denotes the areas impacted above the threshold for surface ecological impacts (1 μm) but below the threshold for surface mortality (10 μm). Computation of subsurface concentrations are limited to the shown black box.

and Richards Bay. The DSD 2 simulaion reveals the three-dimensional characteristics of a meander in the Agluhas Current, commonly known as a Natal Pulse. The results at 60 days after the start of the spill indicate that the oceanographic features of the region are no longer discernible, however a large amount of particles remain within the model domain for both DSD scenarios.

The maximum surface oil thickness, shoreline oil concentration and subsurface oil concentration attained over the extent of this simulation are shown in Figure 4.2 (note these plots indicate the maximum over time computed from 3 hourly time-steps over the duration of the 90 day simulation). The values delineating different colours in Figure 4.2 have been specifically chosen to reflect the socio-economic and ecological thresholds presented in Table 3.1.

The slower oil droplet rise velocities associated with DSD 2 result in predictably lower surface oil concentrations, although both DSD's lead to surface oil thicknesses which exceed 1 μm, used as in indicator for the onset of ecological impacts (top panel of Figure 4.2). Shoreline impacts are significant for both DSD simulations, where the results indicate a large extent of shoreline where the maximum shoreline oil thicknesses are in excess of 100 g m^{-2}, used as an indicator of mortality of seabirds, marine life and organisms associated with the shoreline (middle panel of Figure 4.2). Subsurface concentrations are presented for a limited area of the model domain, as mentioned in Section 3.5.1. The bottom panels of Figure 4.2 provide the maximum concentration attained over time as well as depth. The spatial extent of the impact is predictably larger for the DSD 2 scenario than for DSD 1, however neither simulation resulted in concentrations which exceeded 100 μgl^{-1}, used as an indicator of subsurface impacts (Table 3.1). It should however be noted that the computed concentrations correspond to an average concentration within each 7.5 km x 7.5 km x 50 m grid cell (Section 3.5.1), and therefore subsurface impacts at a smaller spatial scale than this are not captured in this analysis. It should also be stressed that in reality, subsurface impacts are primarily due to the dissolved polyaromatic hydrocarbons (PAHs), which we do not explicitly simulate with the model. Here, we have simply assumed that the dissolved PAH concentration can be approximated by 1% of the total subsurface oil. While this approximation does not flag any subsurface impacts, a more complete depiction of the dissolution process and a finer model grid resolution may show otherwise. Indeed, the dissolution of PAH's was found to lead to significant subsurface impacts in the Deepwater Horizon spill (Berenshtein et al., 2020). The results of

this study therefore focus on the impacts associated with surface and shoreline oiling.

Figures 4.3 and 4.4 present the same model output as shown in Figures 4.1 and 4.2, but for an example simulation which resulted in significant oiling on the south coast of South Africa (in the case of the DSD 1 scenario). For reference, this represents the 89th percentile simulation in terms of shoreline length oiled above the 1 g m^{-2} threshold for DSD 1. In this simulation the surface oil is shown to be rapidly transported down the east coast, which is not at all impacted, however the variability in the current off the south coast causes a significant portion of the released oil to be entrained onto the Agulhas Bank, which enables significant interaction of oil with the south coast (again, only for the DSD 1 scenario). These processes are reflected in the maps of maximum surface oil thickness and maximum shoreline oiling over the simulation (Figure 4.2).

4.2. 15 day blowout: stochastic results

Figures 4.5 to 4.7 present the full set of stochastic results for the east coast 15 day blowout spill scenario. Both the faster and slower rising DSD's are shown, for comparative purposes. The figures are presented as stochastic mass balances (Figure 4.5), spatial maps indicating the probability of surface (Figure 4.6) and shoreline (Figure 4.7) impacts, and exceedance curves for the area swept and shoreline length oiled (Figure 4.8).

The stochastic mass balance (Figure 4.5) confirms that for the faster rising droplet scenario (DSD 1), particles reach the surface very quickly, where more than half of the total mass of oil released is evaporated within a few days of surfacing. The remaining oil-water emulsion is exchanged between the surface and subsurface in response to wind-wave evens (which drive entrainment) and subsequent resurfacing due to oil droplet buoyancy. A relatively small fraction of the total mass of oil released is expected to impact the coastline (up to 20% in the case of the 95th percentile). The mass balance for this simulation is shown to change very little from $\sim$50 days after the start of the spill. The slower rising droplet scenario (DSD 2) indicates predictably higher subsurface oil with commensurately lower surface oil, particularly during the early stages of the spill.

By way of comparison, a recent oil fate modelling study of the Deepwater Horizon spill indicated that $\sim$89% of the total oil released reached the surface, while $\sim$11% of the total

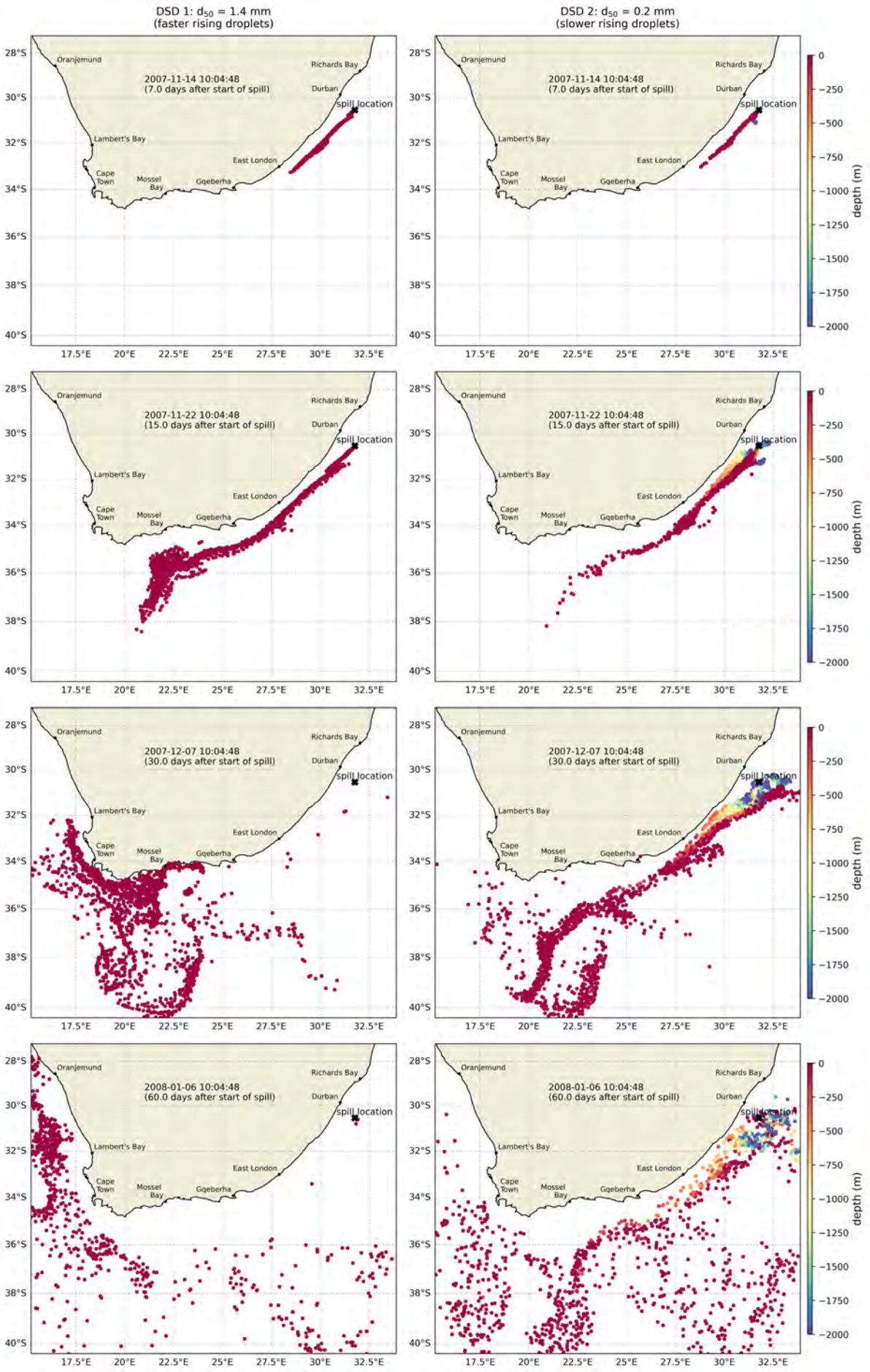

Figure 4.3: East coast 15 day blowout: modelled particle locations at snapshots in time for an example simulation which resulted in significant oiling on the south coast of South Africa.

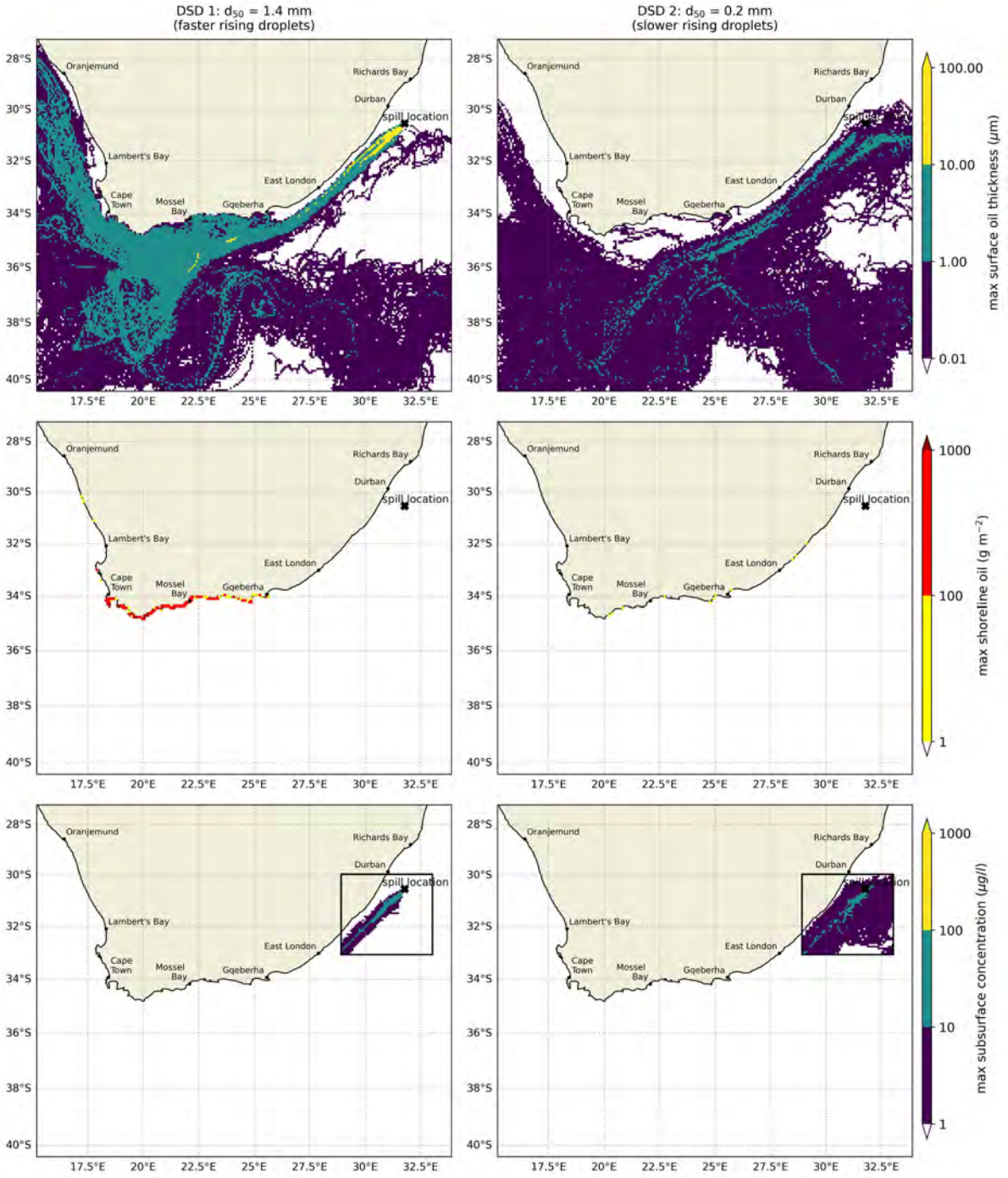

Figure 4.4: East coast 15 day blowout: modelled surface oil thickness (top panels), stranded oil concentration (middle panels) and subsurface oil concentration (bottom panels) for an example simulation which resulted in significant oiling on the south coast of South Africa. The values delineating different colours reflect the consequence thresholds presented in Table 3.1 e.g. the green in the top panels denotes the areas impacted above the threshold for surface ecological impacts (1 μm) but below the threshold for surface mortality (10 μm). Computation of subsurface concentrations are limited to the shown black box.

oil was retained in the subsurface through dissolution or as microdroplets, some of which were biodegraded (French-McCay et al., 2021a). Of the oil which reached the surface, ∼41% evaporated, ∼15% was ashore and in nearshore (<10 m) sediments, ∼3% was removed by responders, ∼38.4% was entrained in the water column and 2.6% sedimented in waters >10 m (French-McCay et al., 2021a).

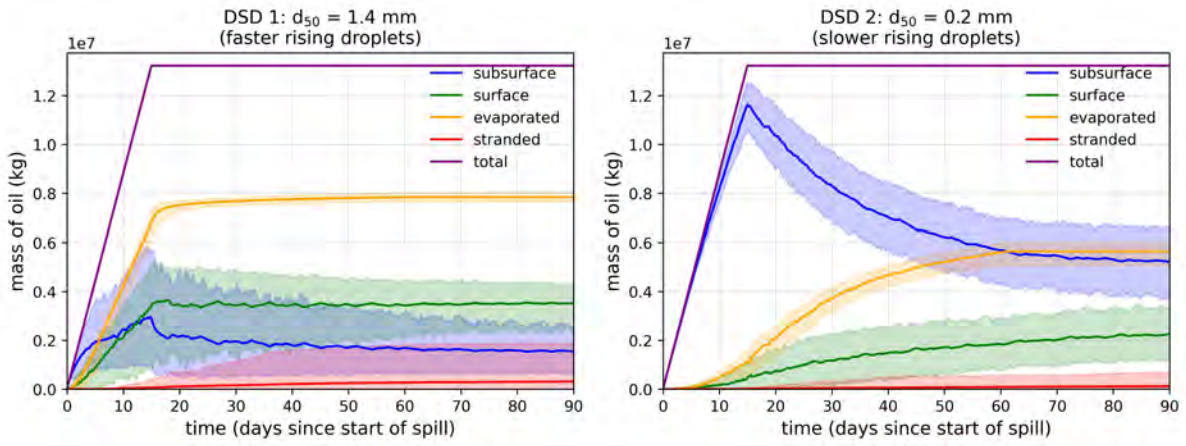

Figure 4.5: East coast 15 day blowout in 2 900 m water depth: stochastic mass balance. Solid lines denote the mean value over all simulations, while the shaded area denotes the range between the 5th and 95th percentile values. The results are computed from a total of 200 simulations.

Figure 4.6 (top panels) indicates that at a surface oil thickness threshold of 0.01 μm, used as an indication of socio-economic impacts (Table 3.1), most of the model domain has at least some risk of impact. This output in fact represents the probability of oiling at any concentration whatsoever, as this threshold is always exceeded if oil is present in the model due to the relatively high mass of oil associated with each particle (even after weathering) relative to the output grid size. The spatial footprint of the areas which might be impacted becomes predictably smaller as the surface oil thickness threshold is increased. At a threshold of 1 μm, used as an indication of the onset of ecological impacts on the surface (Table 3.1), the median (i.e. 50th percentile) spatial extent of the impact area ranges between and 60 000 and 280 000 km^2 for two DSD's (Figure 4.8, orange lines in top panels). Figure 4.6 (bottom panels) indicates that the threshold of 10 μm, used as an indication of mortality of seabirds and other wildlife associated with the ocean surface (Table 3.1), is exceeded in about 60% of simulations for DSD 1, although the spatial extent of the impact at this threshold is low, as highlighted in Figure 4.8 (green line, top panels). The 10 μm threshold is only exceeded in 1% of the simulations for DSD 2, with negligible area of impact.

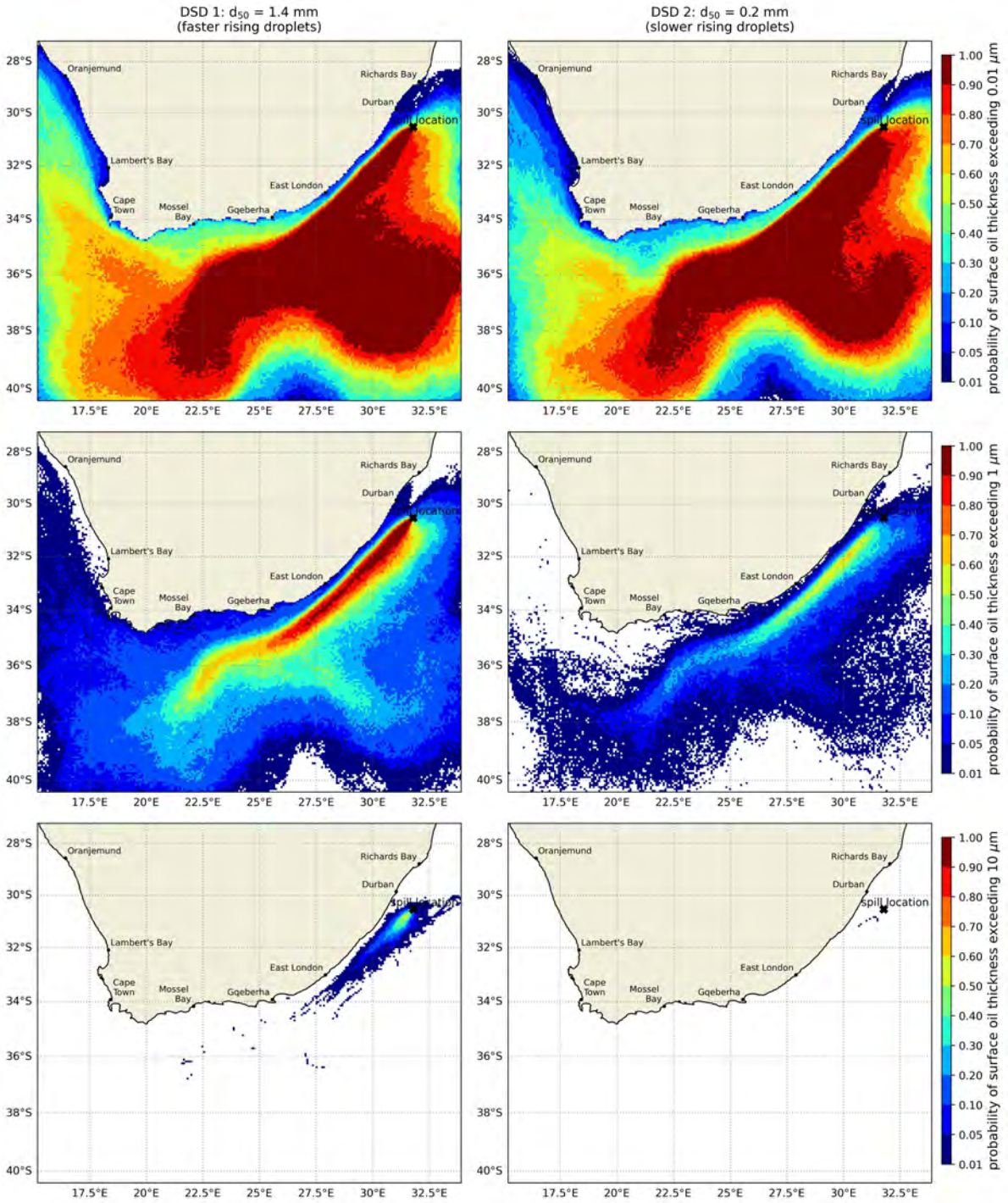

Figure 4.6: East coast 15 day blowout in 2 900 m water depth: stochastic model output for surface oil thickness at different thresholds. The results are computed from a total of 200 simulations, and do not represent the spatial extent of a single simulation/spill event.

The areas of highest probability of impact clearly reflect the features of the Agulhas Current, as described in Section 2.3. The modelled spill location is in close proximity to the origin of the stable northern region of the Agulhas Current (Figure 2.3). As such, oil released into the ocean at this location is transported over great distances, predominantly driven by variability

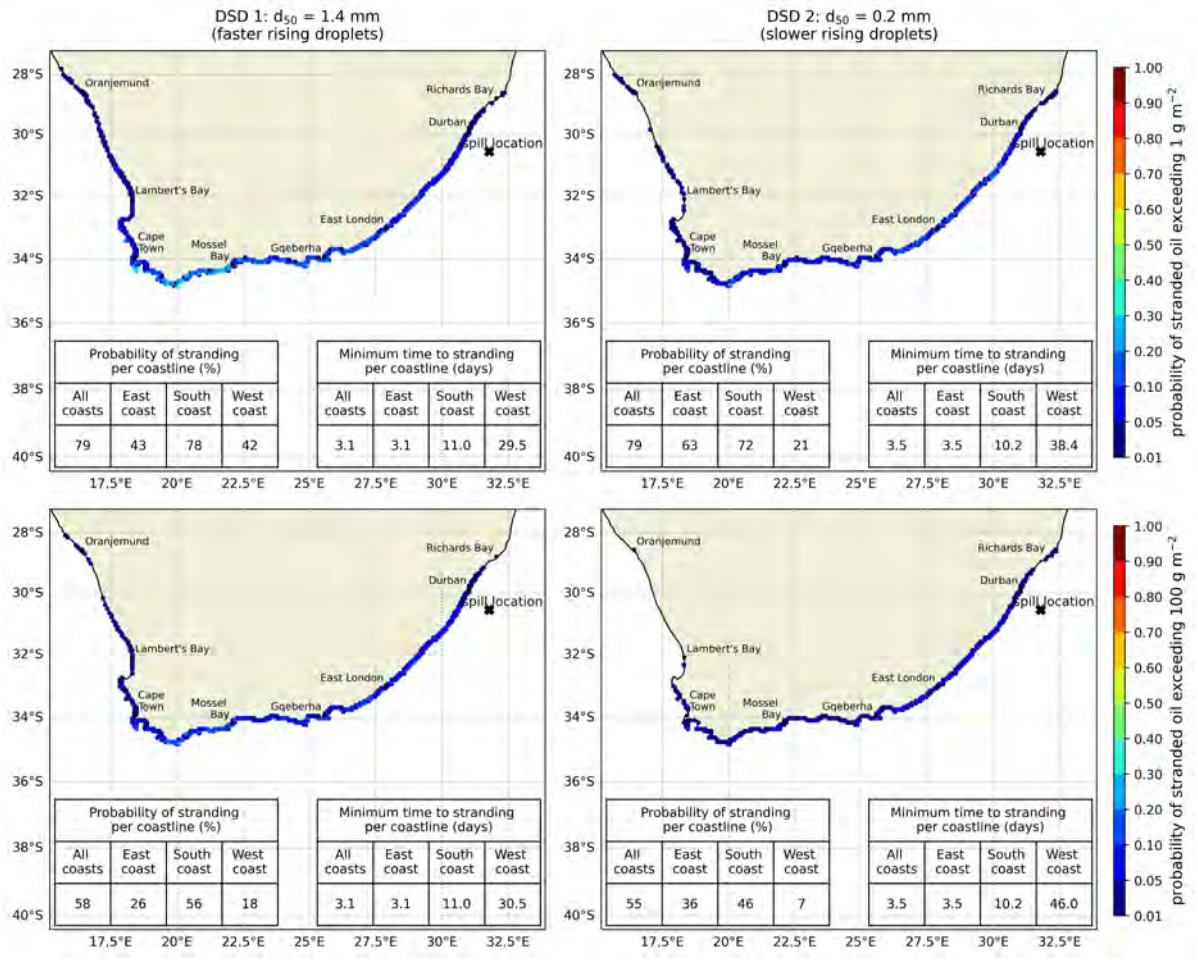

Figure 4.7: East coast 15 day blowout in 2 900 m water depth: stochastic model output for stranded oil concentration at different thresholds. The results are computed from a total of 200 simulations, and do not represent the spatial extent of a single simulation/spill event.

of the currents, but also by surface winds. As discussed in Section 2.3, the Agulhas Current is relatively stable along the east coast, and therefore the spilled oil from simulations at different start times tend to follow similar trajectories, regardless of the time of the spill. This leads to relatively high probabilities of impact for a long swath down the east coast of South Africa (greater than 90% probability of surface oiling over the 1 μm threshold all the way down to offshore Gqeberha for the DSD 1 scenario. South of Gqeberha, the current becomes more variable (Figure 2.4), and oil can be transported via multiple pathways. Most of the surface oil is shown to be transported into the southern Indian Ocean via the Agulhas retroflection and return current, although oil can be entrained onto the Agulhas Bank and/or transported into the Atlantic Ocean via the Agulhas leakage. The results therefore indicate relatively strong connectivity between the modelled spill location and the surface waters off the west coast of South Africa, with an estimated probability of surface oiling here of $\sim$40-60% at the 0.01 μm

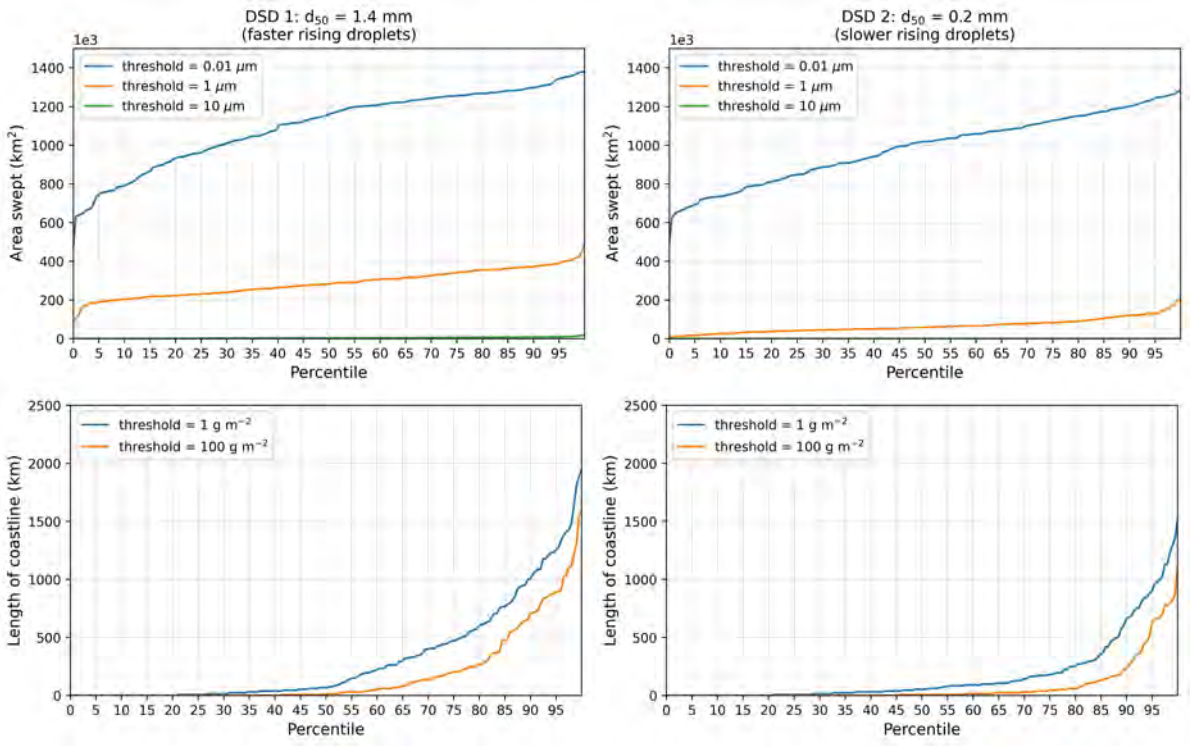

Figure 4.8: East coast 15 day blowout in 2 900 m water depth: exceedance curves for area swept by surface oil (top panels) and shoreline length oiled (bottom panels) at different thresholds. The results are computed from a total of 200 simulations.

threshold, reducing to ∼1-10% at the 1 μm threshold (top panels of Figure 4.6, DSD 1 scenario).

The transport of oil as described above naturally dictates where oil is likely to make contact with the shoreline. Figure 4.7 indicates that at a concentration of 1 gm^{-2}, used to indicate the need for a beach cleanup (Table 3.1), almost the entire coastline of South Africa is under at least some risk of shoreline impact for both droplet size distribution scenarios, although the shown probabilities are low for any specific location due to the variability in where the various spill simulations contact the shoreline (typically less than 20% over much of the coastline, but up to a maximum of 35%). It is however important to note that each data point (i.e. the coloured dots shown in Figure 4.7) represents a 7.5 km stretch of coastline, and so the plot indicates the probability of oiling for any particular 7.5 km stretch of coastline. Also provided in Figure 4.7 however are tables which indicate the probabilities of shoreline impacts for east, south and west coasts, as well as for any coastline in the shown model domain (Cape Town and Gqeberha are used as the points which separate the different stretches of coastline). These summary tables indicate that there is estimated to be a 79% probability that a beach

cleanup will be required at some location (coincidentally the same probability under both DSD scenarios), while there is a 55-58% probability that shoreline oiling would exceed the threshold for mortality of organisms associated with the shoreline in at least one location (the range considers both DSD scenarios).

It is interesting to note that the south coast has a far higher probability of shoreline impact when compared to the east coast. For example, the south coast is estimated to have a 78% chance of at least some impact at a threshold of 1 gm^{-2} for DSD 1, which reduces to 43% for the east coast (top left panel of Figure 4.7). Indeed, the maximum probability of oiling at any specific location is 36% and is in close proximity to Cape Agulhas, located on the southern tip of Africa. This may seem counter-intuitive, given the location of the spill, however the relative stability of the Agulhas Current, as previously described, serves to maintain oil within the core of the current along the east coast, while higher variability south of Gqeberha serves to sweep oil onto the Agulhas bank, where the predominant winds (Figure 2.9) would aid in oiling on the southern extent of the continent, where shoreline probabilities are in fact shown to be highest. The strong connectivity between the east and west coast oceanographic features is again highlighted in the shoreline oiling results for the west coast, which are surprisingly high. Figure 4.7 indicates probabilities of impact ranging from 42% at a threshold of 1 gm^{-2} for DSD 1 down to 7% at a threshold of 100 gm^{-2} for DSD 2.

Also provided in Figure 4.7 are estimates of the minimum time to stranding per coastline. Given the modelled spill location, the lowest response time corresponds to the east coast, where oil can make contact with the shoreline in the order of 3 days. The minimum time to oiling for the south coast increases to about 10 days, while oil would take a minimum of about a month to reach the west coast. These estimates provide some insight into the response time requirements for land-based clean-up operations in the event of a spill. The long transit time for oil to reach the west coast illustrates the importance of running model simulations for a sufficient duration such that the ultimate fate and transport of spilled oil is accurately reflected. This is especially important for spill scenarios where a large portion of the spilled oil is expected to be entrained in the water column, as this oil is still subject to transport and can resurface during periods of weaker currents/winds.

The lower panels of Figure 4.8 provide insight into the length of coastline which is estimated to be impacted under the different thresholds. While the length of coastline impacted at the

1 gm^{-2} threshold is estimated to be less than 100 km with a 50% probability (i.e. at the 50^{th} percentile), the maximum modelled shoreline length oiled in a single spill simulation is about 1 800 km. For reference, this is about the distance along the shoreline from Cape Town to Richards Bay, but it should be noted that an event such as this would have a low probability of occurrence (1 in 200 as estimated in the model).

4.3. 60 day blowout: stochastic results

Figures 4.10 to 4.11 provide the same stochastic model output as shown for the 15 day blow-out scenario (Figures 4.5 to 4.7), but for the 60 day blow-out scenario. No further explanation for these figures is provided, as the text from Section 4.2 is largely applicable. All of the impacts are however predictably larger, given that four times as much oil is released into the model over a spill duration which is four times longer. This enables oil to be transported in more pathways over the duration of each simulation, and at higher concentrations. By way of comparison, for the 15 day blowout scenario it is estimated that there is a 55-58% probability that shoreline oiling would exceed the threshold for mortality of organisms associated with the shoreline (the range considers both DSD scenarios), while these values increase to 78-79% for the 60 day blowout scenario.

4.4. Sensitivity to season

Here, we again present the results of the 15 day east coast blowout scenario, but consider the time of year in which the start of the modelled spills occur. We take the months of April to September to represent nominally winter months, while nominally summer months are taken as October to March. This limits the stochastic analysis to 100 simulations in each season. Figures 4.15 to 4.14 compare the stochastic results of these two periods of the year, considering only DSD 1 i.e. the faster rising droplet scenario.

The results indicate that the time of the year in which the east coast blowout takes place has a significant effect on the ecological risks, particularly with respect the shoreline impacts. As shown in Section 2.4, the near-coastal winds around Southern Africa tend to be shore parallel, with easterly winds becoming more prevalent in summer months (Figure 2.9). Figure 4.13 clearly indicates that summer months result in a significantly higher probability of oil being

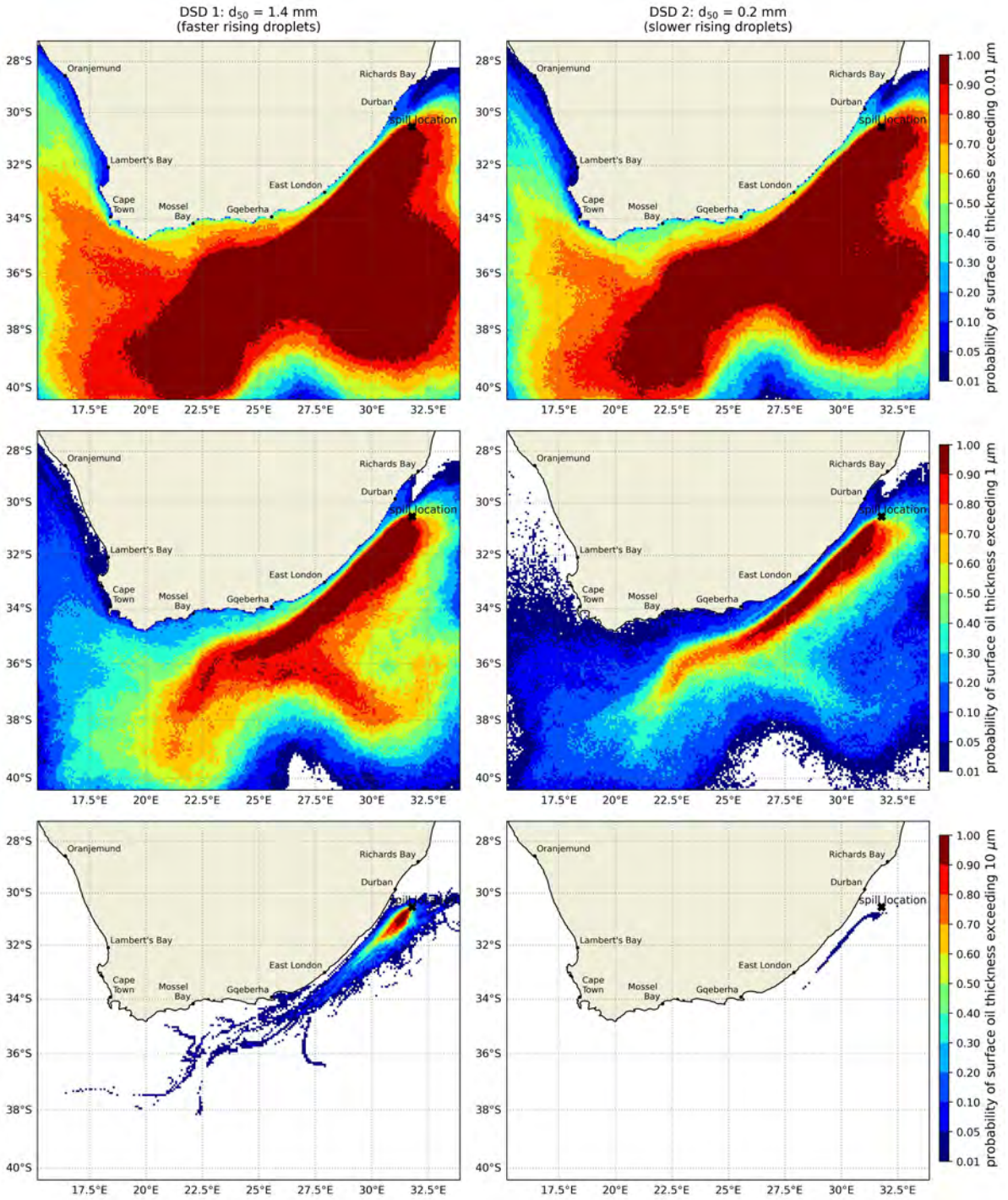

Figure 4.9: East coast 60 day blowout in 2 900 m water depth: stochastic model output for surface oil thickness at different thresholds. The results are computed from a total of 200 simulations, and do not represent the spatial extent of a single simulation/spill event.

entrained onto the Agulhas Bank off the south coast, which is attributed to the enhanced easterly winds in the region at this time of the year. Shoreline impacts are consequently greater in summer months than in winter (Figure 4.14). For example, it is estimated that the south coast has a 94% probability of shoreline concentrations exceeding 1 gm^{-2} during the nominally

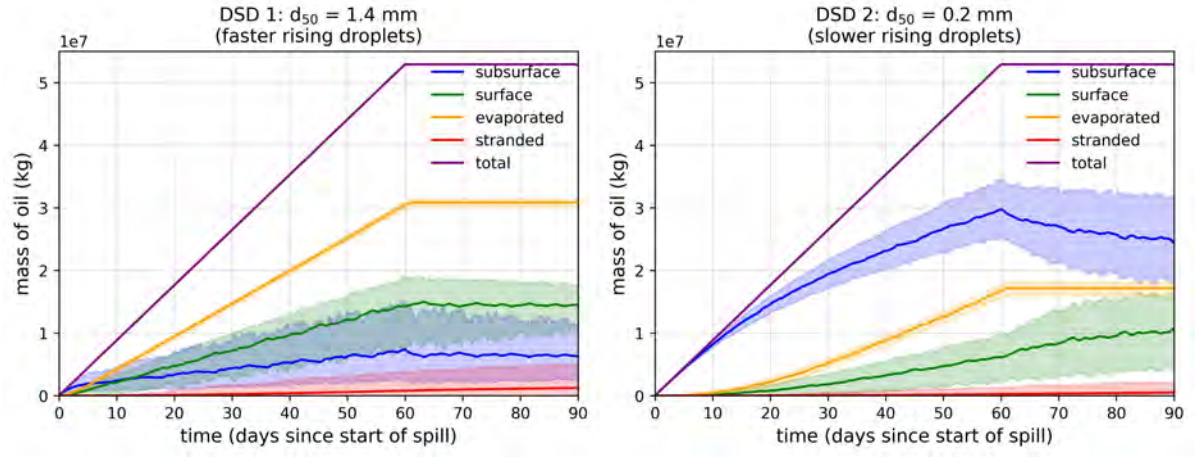

Figure 4.10: East coast 60 day blowout in 2 900 m water depth: stochastic mass balance. Solid lines denote the mean value over all simulations, while the shaded area denotes the range between the 5th and 95th percentile values. The results are computed from a total of 200 simulations.

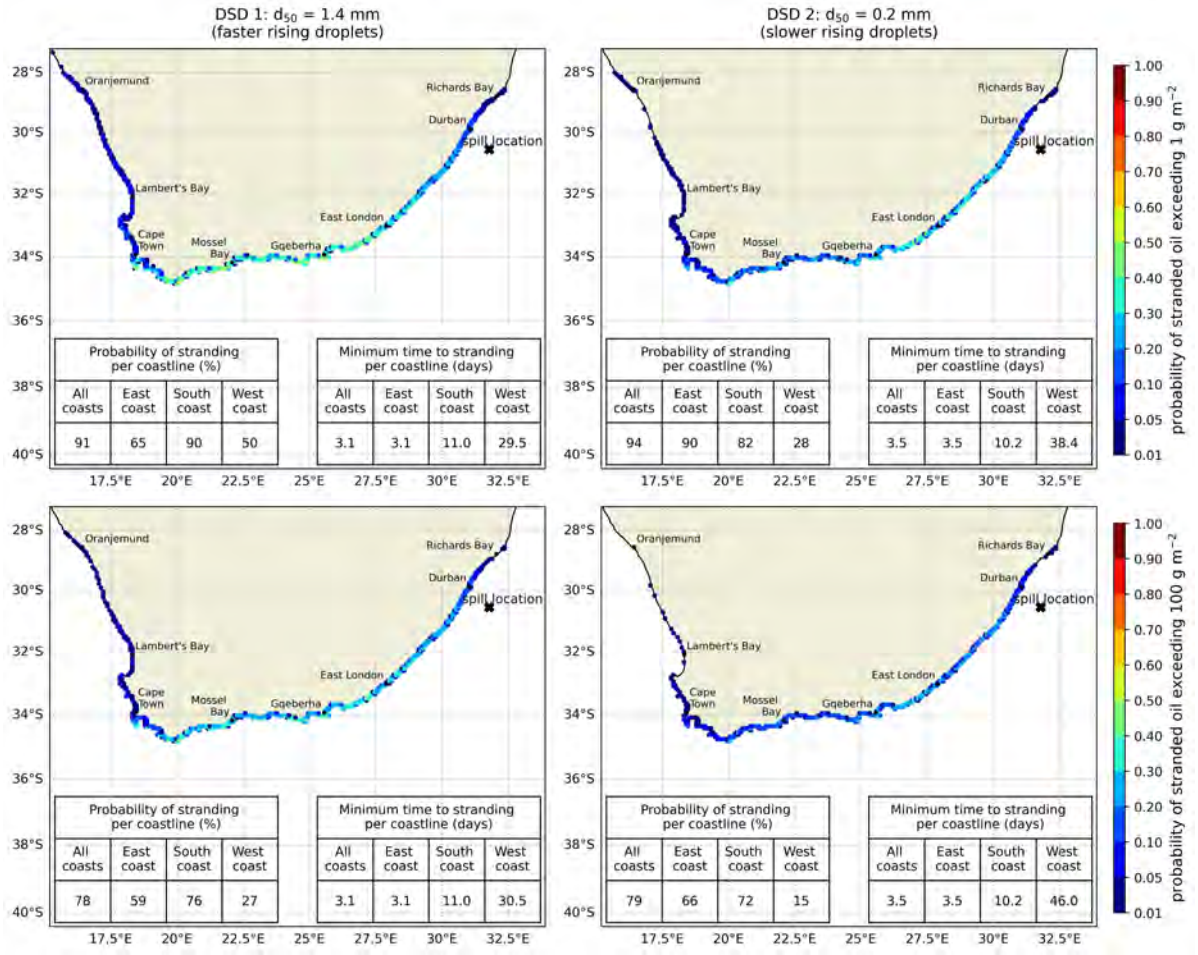

Figure 4.11: East coast 60 day blowout in 2 900 m water depth: stochastic model output for stranded oil concentration at different thresholds. The results are computed from a total of 200 simulations, and do not represent the spatial extent of a single simulation/spill event.

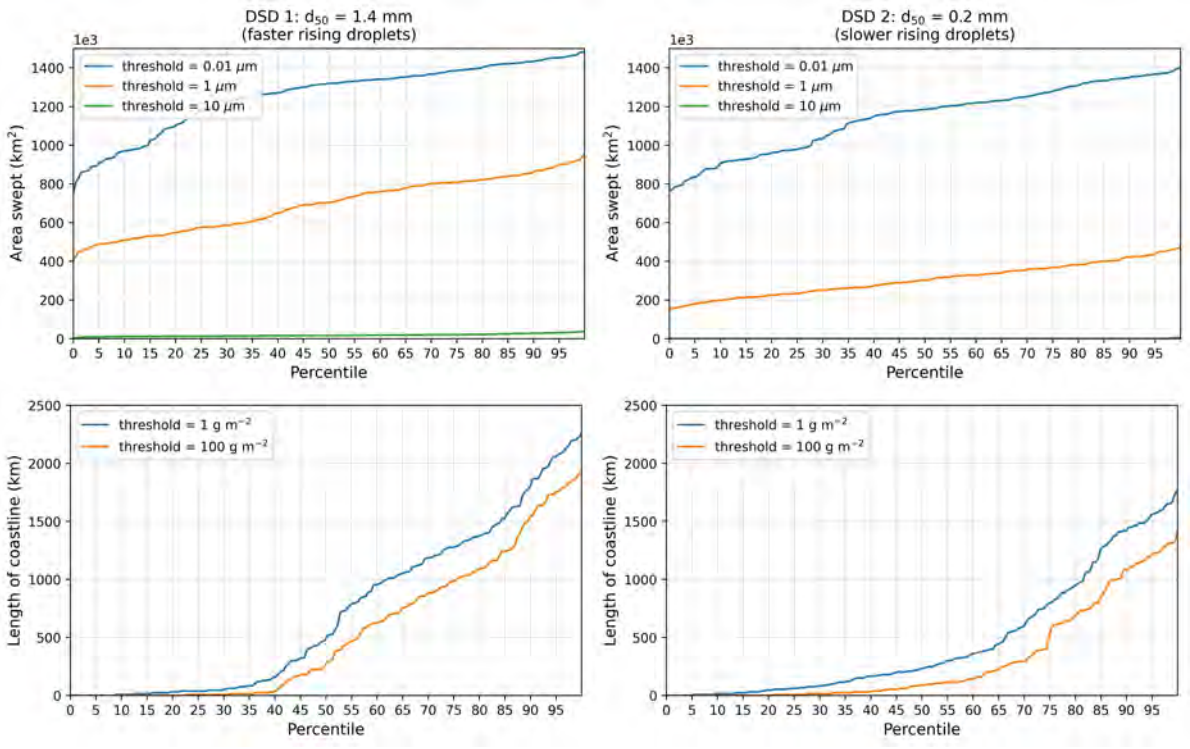

Figure 4.12: East coast 60 day blowout in 2 900 m water depth: exceedance curves for area swept by surface oil (top panels) and shoreline length oiled (bottom panels) at different thresholds. The results are computed from a total of 200 simulations.

summer months (with a maximum of 57% for a specific location), reducing to a 64% probability in nominally winter months (with a maximum of 16% for a specific location).

4.5. Sensitivity to ocean model resolution

In Section 2 we introduced three ocean models which could be used as input to the oil spill model; namely a ∼7.5 km resolution global ocean reanalysis (GLORYS) and two domains from a CROCO regional simulation with resolutions of ∼7.5 km and ∼2.5 km, respectively. The results presented until now have been based on current input from the CROCO 2.5 km resolution domain, having been selected for its favourable comparison with the available observations and the higher spatial resolution offered by this product.

We now compare the stochastic results from the oil spill model from simulations forced by both the CROCO 2.5 km and 7.5 km domains (Figures 4.18 to 4.17). As per the seasonal sensitivity test, we only present results for the faster rising oil droplet scenario (DSD 1). The presented comparison is considered important as the limited spatial extent of the 2.5 km resolution domain prohibits its used as input for simulations which consider spills off the south and

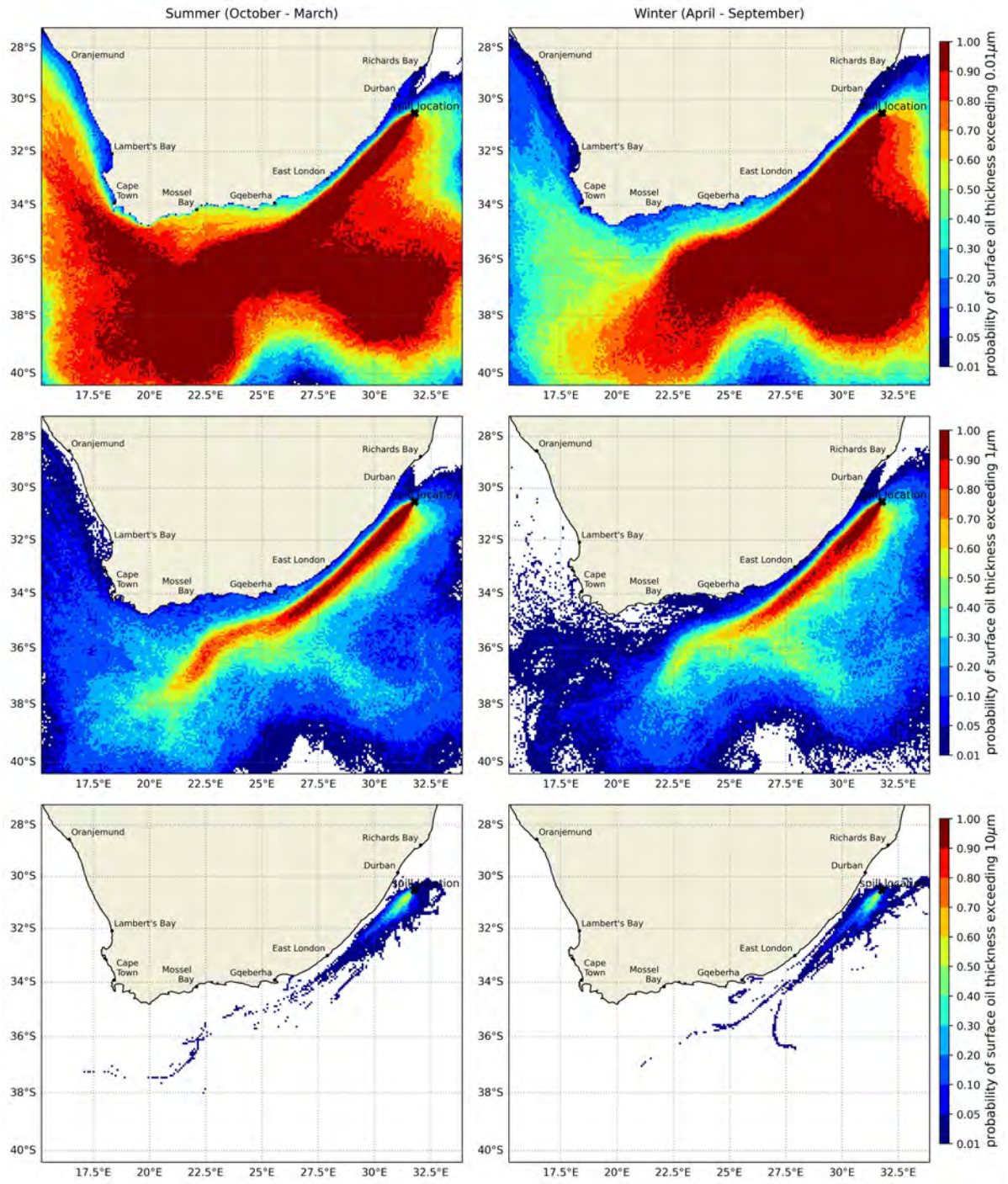

Figure 4.13: East coast 15 day blowout in 2 900 m water depth assuming DSD 1 (faster rising droplets): seasonal sensitivity in stochastic model output for surface oil thickness at different thresholds. The results are computed from a total of 100 simulations, and do not represent the spatial extent of a single simulation/spill event within each season.

west coasts of South Africa (Section 4.6). and so we are required to use the 7.5 km resolution domain for these simulations (Figure 2.1).

The stochastic results from using the two different resolution domains are shown to be generally similar, although some differences can be identified. Notably, the results from the

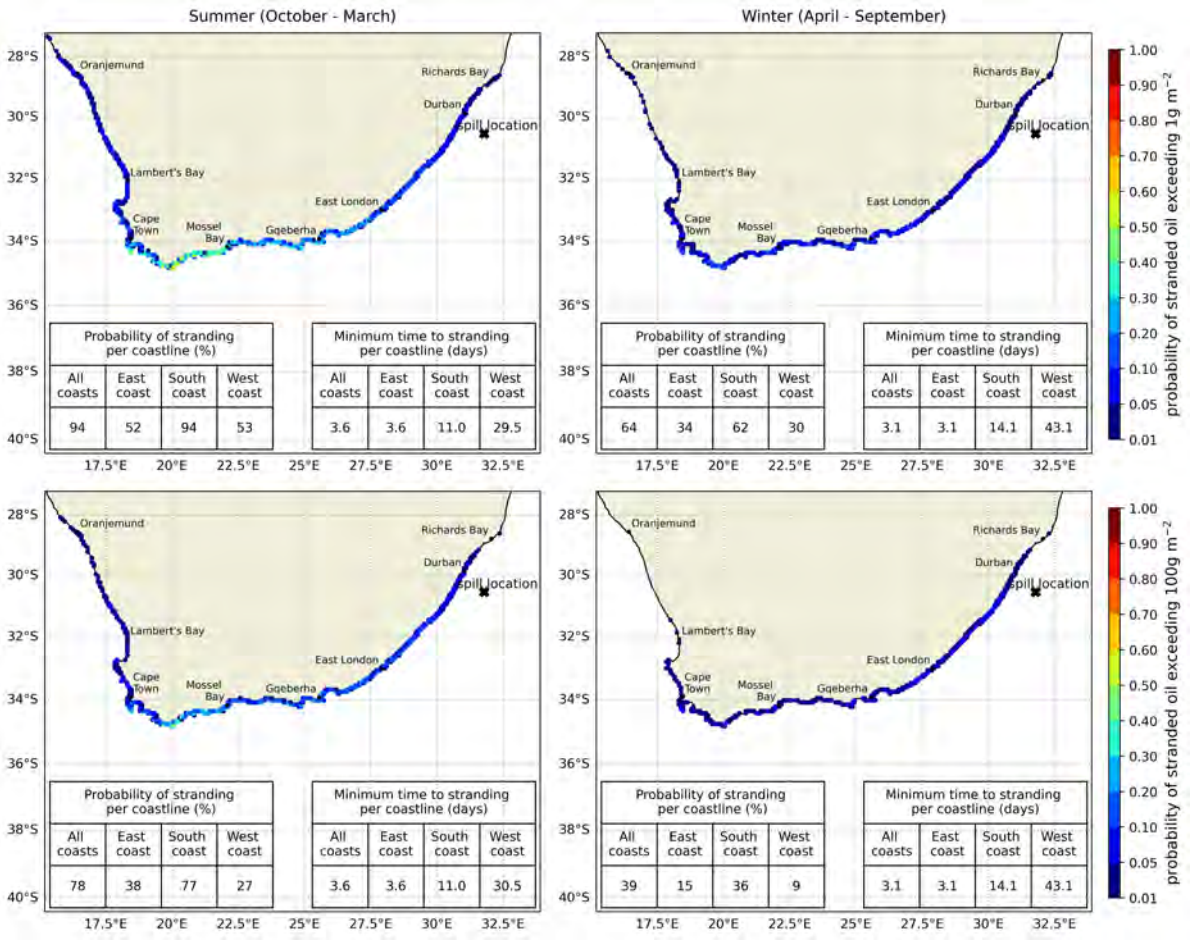

Figure 4.14: East coast 15 day blowout in 2 900 m water depth assuming DSD 1 (faster rising droplets): seasonal sensitivity in stochastic model output for stranded oil concentration at different thresholds. The results are computed from a total of 100 simulations, and do not represent the spatial extent of a single simulation/spill event within each season.

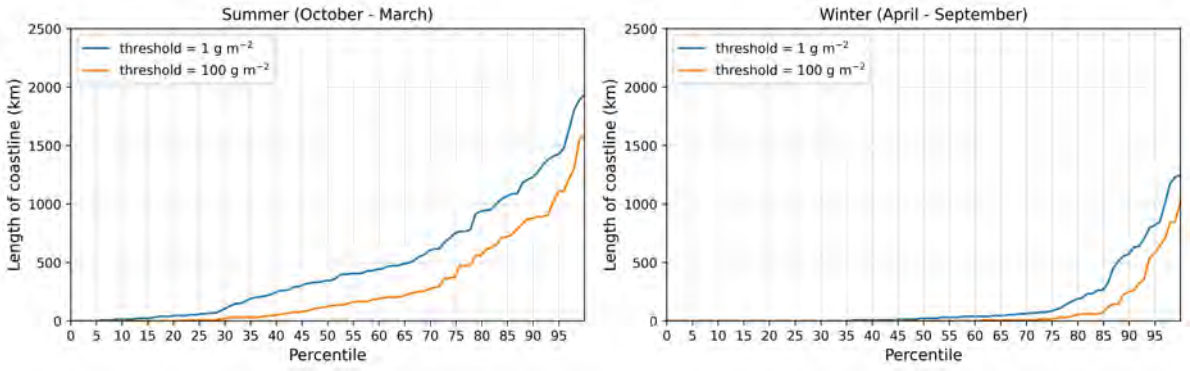

Figure 4.15: East coast 15 day blowout in 2 900 m water depth assuming DSD 1 (faster rising droplets): seasonal sensitivity in exceedance curves for shoreline length oiled at different thresholds. The results are computed from a total of 100 simulations within each season.

2.5 km domain lead to more entrainment of oil onto the Agulhas Bank, and therefore higher probabilities of shoreline impact. For example, the probability of shoreline oiling over the threshold of 1 gm^{-2} on the south coast is 78% when the 2.5 km resolution domain is used

(with a maximum of 36% for a specific location), which reduces to 68% when the 7.5 km resolution domain is used (with a maximum of 26% for a specific location). The probabilities of shoreline impacts are similarly larger for the estimated west coast shoreline impacts, due to the same processes. The higher resolution ocean model however appears to marginally reduce shoreline oiling on the east coast, which could be explained by the relative stability of the Agulhas Current here, and a higher resolution representation of the current tending to maintain oil further from the coast.

4.6. Sensitivity to spill location

We now consider blowout spills from potential locations off the south and west coasts of South Africa. As explained in Section 3.1, we keep the spill scenario the same in each (despite certain differences between flow rates and oil types at the different well sites), so that we can isolate the effect of the varying oceanographic and atmospheric features on the trajectory of a hypothetical oil spill from different locations. The 7.5 km CROCO model domain (Figure 2.1) is used as ocean input to the model, given the larger spatial coverage required for the experiment. Figure 4.19 compares the probability of surface oil thickness exceeding 1 μm for releases at the three locations, while the probability of shoreline oiling over 1 gm^{-2} is shown in Figure 4.20. Shoreline impacts are further compared through exceedance curves of the length of shoreline oiled (Figure 4.21).

While the south coast blowout spill is shown to place less of a risk to the east coast (shoreline oiling is not expected to occur at all north of East London), the stretch of coastline from Cape Agulhas (the southern tip of the continent) to Cape Columbine (the prominent headland between Cape Town and Lambert's Bay) has a particularly high probability of impact. The model estimates a 86% probability of shoreline impact above the threshold for beach cleanup operations, with a maximum probability at any specific location of 76%, being associated with the Cape Peninsula (just south of Cape Town). Furthermore, the south coast spill is shown to lead to the oiling of longer stretches of coastline than the east coast spill, although the maximum oiled length of coastline is similar for both, as indicated in Figure 4.21.

The south coast spill location is roughly coincident with the start of the northward flowing Benguela Current, which in its mean state is comprised of two main streams (Veitch et al.,

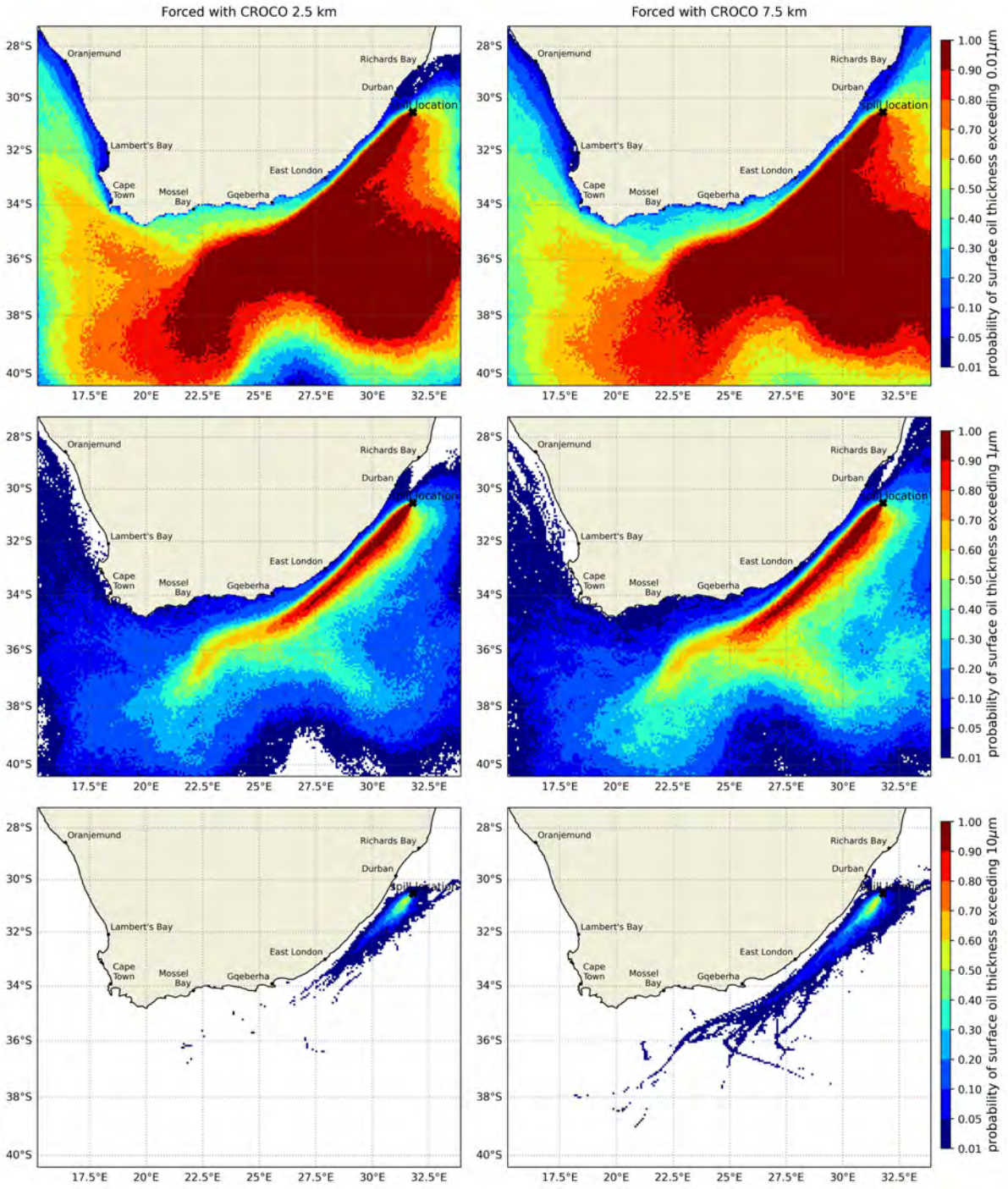

Figure 4.16: East coast 15 day blowout in 2 900 m water depth assuming DSD 1 (faster rising droplets): sensitivity to ocean model resolution in stochastic model output for surface oil thickness at different thresholds. The results are computed from a total of 200 simulations, and do not represent the spatial extent of a single simulation/spill event.

2010). The offshore stream is dictated by the preferential path of Agulhas Rings and eddies (Veitch and Penven, 2017) while the inshore stream (known as the Benguela Jet or Goodhope Jet) is predominantly driven by cross-shore density gradients set up by seasonally varying upwelling, and typically follows the edge of the continental shelf (Veitch et al., 2018). The

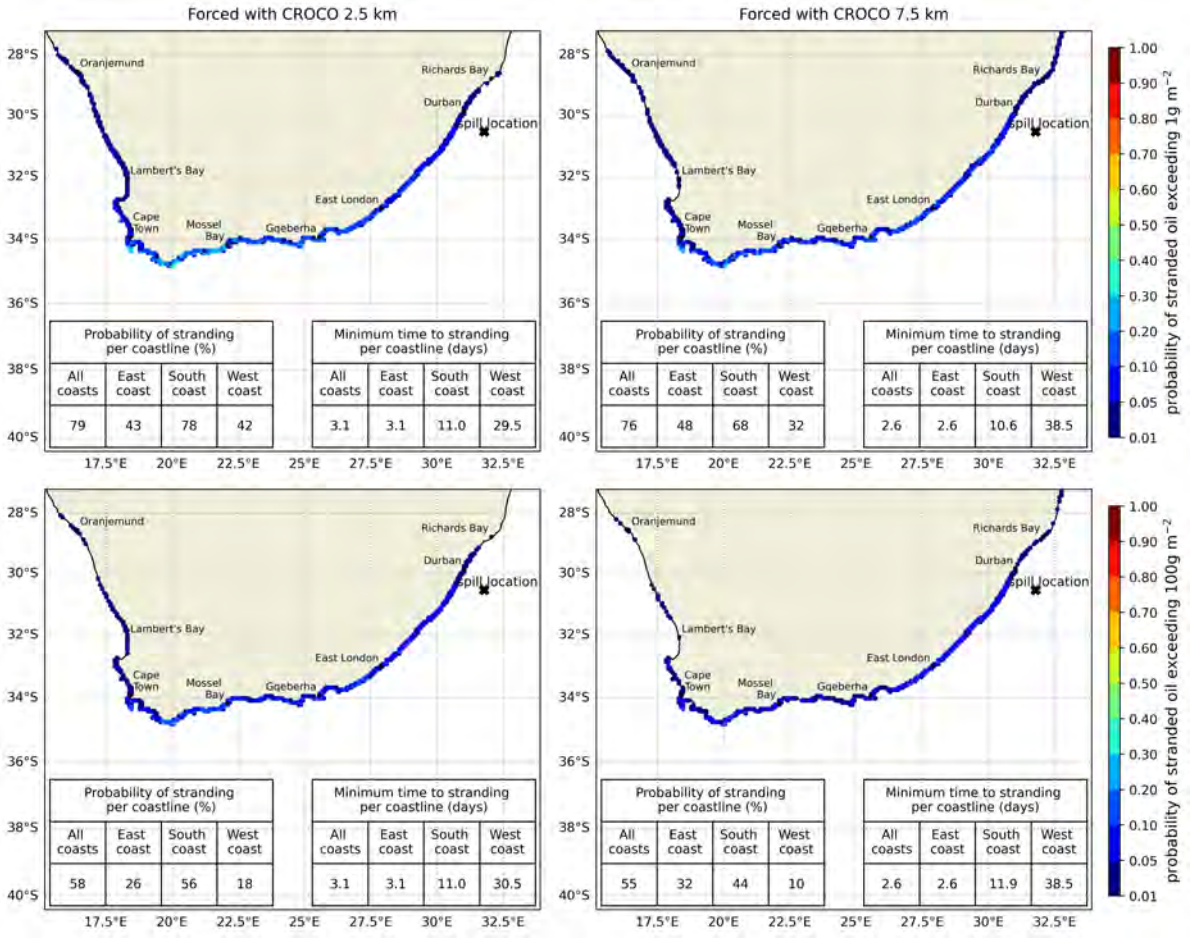

Figure 4.17: East coast 15 day blowout in 2 900 m water depth assuming DSD 1 (faster rising droplets): sensitivity to ocean model resolution in stochastic model output for stranded oil concentration at different thresholds. The results are computed from a total of 200 simulations, and do not represent the spatial extent of a single simulation/spill event.

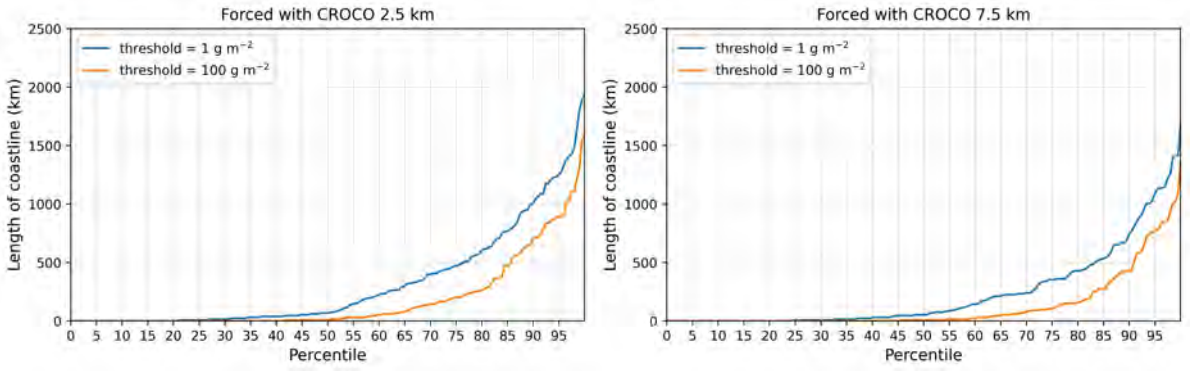

Figure 4.18: East coast 15 day blowout in 2 900 m water depth assuming DSD 1 (faster rising droplets): sensitivity to ocean model resolution in exceedance curves for shoreline length oiled at different thresholds. The results are computed from a total of 200 simulations.

Goodhope Jet has been identified as a key factor in transporting fish eggs and larvae from their spawning ground on the Agulhas Bank to their nursery area in St Helena Bay on the west coast (Ragoasha et al., 2019). The modelled spill location is shown to be largely influenced by

this oceanographic pathway, as well as generally shore parallel winds, which can maintain oil in close proximity to the coast where it can make contact with the shoreline with the relatively high probability.

Of the three considered spill locations, the modelled west coast location reveals relatively lower probability of shoreline impact (13%), which the model estimates to occur in the region of Oranjemund, near the border between Namibia and South Africa. Here, the spill location is largely under the influence of a sluggish equatorward mean flow, and highly persistent equatorward winds (Figure 2.9). The perennial upwelling cell off Luderitz ($\sim$27°E) would further tend to drive net offshore surface flow in this region. These environmental forcings tend to advect the spilled oil offshore north of Oranjemund and into the Atlantic Ocean.

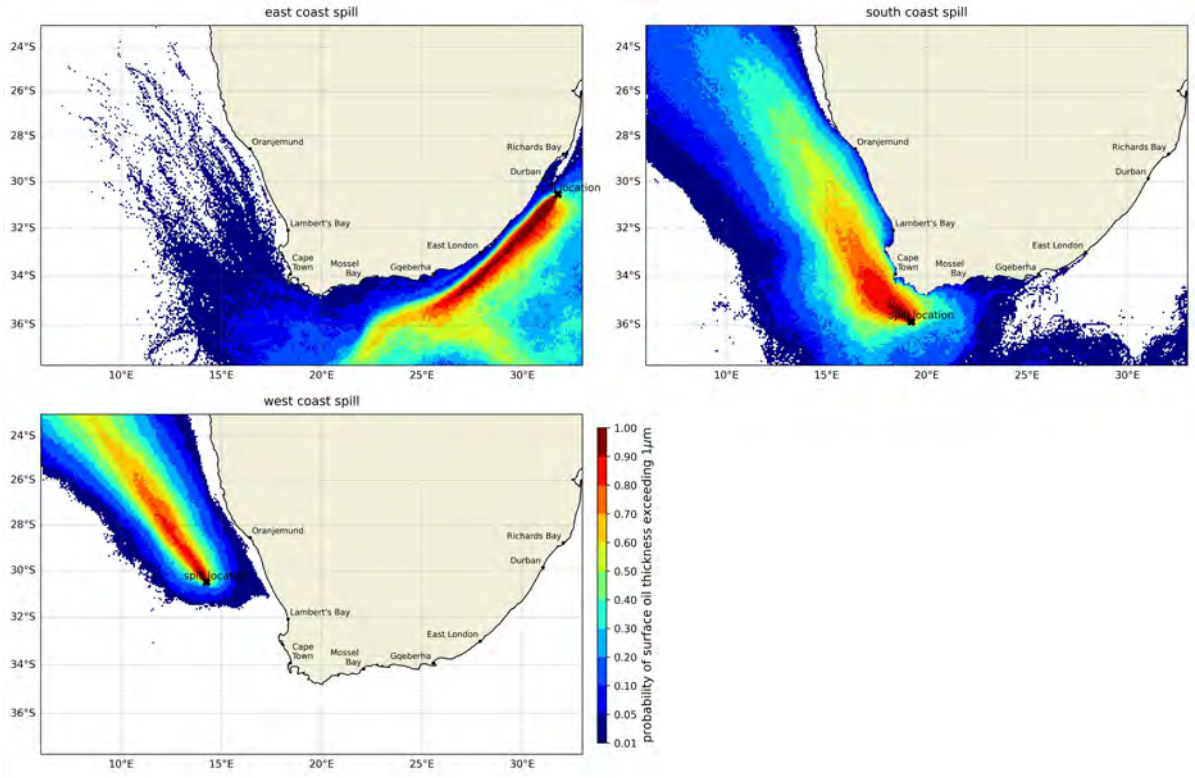

Figure 4.19: 15 day blowout assuming DSD 1 (faster rising droplets): Probability of surface oil thickness exceeding 1 μm for releases at the three locations. The results are computed from a total of 200 simulations, and do not represent the spatial extent of a single simulation/spill event.

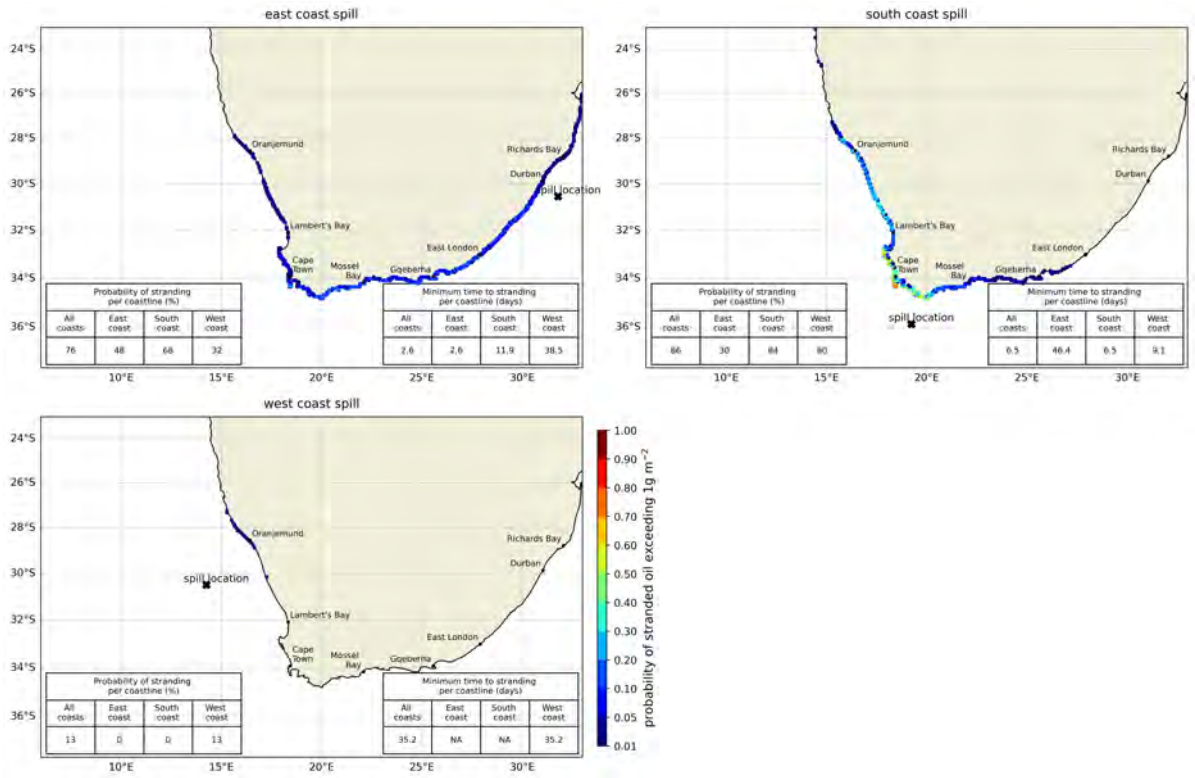

Figure 4.20: 15 day blowout assuming DSD 1 (faster rising droplets): Probability of stranded oil concentration exceeding 1 gm^{-2} for releases at the three locations. The results are computed from a total of 200 simulations, and do not represent the spatial extent of a single simulation/spill event.

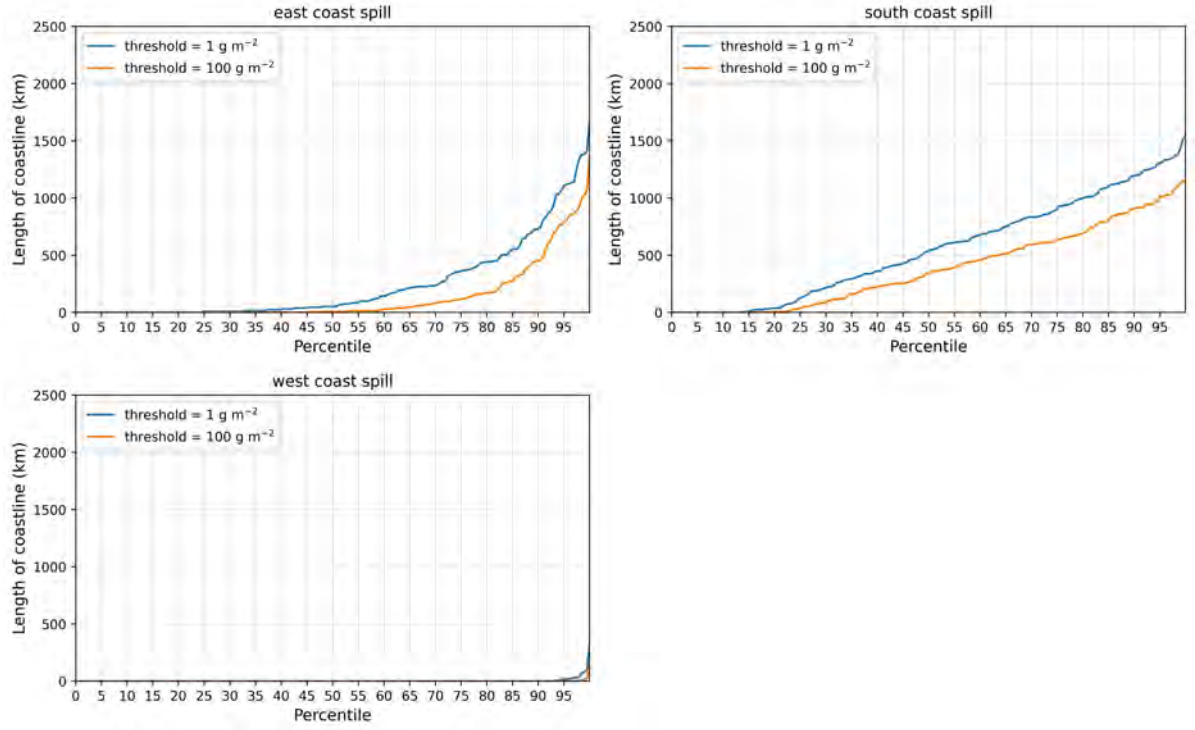

Figure 4.21: 15 day blowout assuming DSD 1 (faster rising droplets): Exceedance curves for length of shoreline oiled over different thresholds for releases at the three locations. The results are computed from a total of 200 simulations.

5

Discussion and conclusions

The oceanographic environment within South Africa's EEZ is complex, dominated by the Agulhas Current off the east and south coasts, and by the Benguela Upwelling System off the west coast. The results of this study have highlighted how the trajectory and fate of potential deep-water blowout spills are largely dominated by the flow pathways of these systems, in concert with highly seasonal surface wind variability.

The transport and fate of oil from a blowout spill on the east coast of South Africa has been shown to be largely dictated by the variability Agulhas Current, which is spatially bi-modal in that the region upstream of Gqeberha is relatively fast flowing and stable, while downstream of Gqeberha it becomes less intense but more unstable (Figures 2.3 and 2.4). The instabilities in the current downstream of Gqeberha, particularly in the form of cyclonic eddies which occur along the inshore edge of the Agulhas Current (Krug et al., 2017; Tedesco et al., 2019) drive the entrainment and retention of oil onto the continental shelf where the predominant winds in the region aid in shoreline oiling. These processes are invoked as an explanation for the surprising result that a 15 day blowout of light crude oil off the east coast of South Africa is estimated to have a 78% probability of shoreline oiling above the 1 gm^{-2} threshold for clean-up operations on the south coast (between Cape Town and Gqeberha), while the east coast has a lower (although still high) 43% probability of oiling. The specific location on the coastline which is predicted to be at greatest risk of impact above the 1 gm^{-2} threshold is Cape Agulhas, on the southern tip of the continent, with a 36% probability of impact. Once oil is entrained onto the Agulhas Bank, the known strong connectivity between this region and coastal regions of west coast of South Africa (Ragoasha et al., 2019) can lead to shoreline oiling on the west coast with a relatively high probability of 41%, although these events would impact a far smaller

shoreline length and at lower concentrations than the east coast shoreline oiling events.

The model results for the 15 day east coast blowout scenario have highlighted the vast distances which oil could be transported. It is envisaged that this, together with a rapid response time requirement (the minimum time to shoreline oiling is $\sim$3 days), would pose significant challenges to a coordinated clean-up effort in the event of a blowout spill off the east coast. An anecdotal example which illustrates this point was the spill of approximately two billion ”Nurdles” (tiny plastic pellets) from a container ship in the Durban Harbour in 2017, which resulted in Nurdle sightings on beaches by members of the public which extended over 2000 km of the South African coastline over a period of 8 weeks (Schumann et al., 2019). Such a spill provides a reasonable template for revealing the oceanographic pathways which oil may take in the event of an east coast blowout spill, which are in good agreement with the findings of this study.

Sensitivity tests to both season and ocean model resolution indicate that, in general, processes which lead to enhanced entrainment of oil onto the Agulhas Bank lead to higher shoreline impacts on both the south and west coasts of South Africa. Summer tends to be associated with elevated easterly winds which increase shoreline impacts when compared with winter spills. Higher resolution ocean models include more entrainment of oil onto the Agulhas Bank through their inclusion of more sub-mesoscale variability in the form of cyclonic eddies along the inner edge of the Agulhas Current. It should however be noted that while the 2.5 km resolution CROCO model adopted for the east coast blowout simulations does include some sub-mesoscale variability, it by no means captures the true nature of the turbulence on the inner edge of the current. It is therefore possible that the use of even higher resolution ocean models may indicate even higher shoreline impacts through a more thorough representation of these processes in the model.

A comparison between blowout spills at different locations (east coast, south coast and west coast) unsurprisingly indicates that the different locations pose very different risks of impacts. Of the three considered locations, the south coast location results in the highest risk of shoreline impact, with an estimated 86% chance of a 15 day blowout needing beach clean-up operations.

In Section 3.2 it was noted that the model employed in this study does not include certain weathering processes such as dissolution, biodegradation and photo-oxidation, which would

add a level of conservatism to the results. It is however argued that these assumptions should be viewed in light of the large uncertainties in defining the spill scenarios. In the face of large uncertainty such as this, the guiding principle should be one of conservatism, which is the approach followed in this study.

Finally, it should be noted that the probabilities presented in this report refer to the probabilities of impact given a potential blowout spill scenario. We have made no mention of the probability that the modelled blowout spill scenarios will actually occur. The true risk of impact would be the probabilities presented in this report multiplied by the probability that the modelled spill scenario will occur during the lifetime of the proposed exploratory and production drilling.

In reality, the risk of a specific blowout scenario would depend on many factors, including the number of exploratory/production wells drilled, the duration of the drilling activities, the well depth, pressure, substrate characteristics, and source control measures such as blowout preventers, capping/containment technologies, and relief wells. The probability of occurrence for a given blowout scenario can be computed using Monte Carlo techniques based on historical blowout data (Etkin, 2015). It has however been argued that the frequency of large blowouts such as the Deepwater Horizon disaster are likely going to increase as the oil and gas industry targets wells in deeper and deeper waters (Murawski et al., 2020). The extreme oceanographic environment, particularly off South Africa's east coast, would further contribute to an increased likelihood of a large blowout, and would create an environment where source control measures would be difficult to implement.

Acknowledgements

The authors would like to thank the WILDTRUST, who initiated the project, through funding from the Energy Transition Fund, as well as Drs Jean Harris, Kendyl Wright and Jennifer Olbers (WILDTRUST) and Prof Mandy Lombard (Nelson Mandela University) who provided advice and comments on the final report. We also thank Dr Jennifer Veitch (South African Environmental Observation Network) who facilitated the sourcing of the CROCO model output used in this study, and Cristina Russo (Department of Forestry, Fisheries and the Environment) who provided assistance in the analysis of the ACT array data.

References

Ainsworth, Cameron et al. (Jan. 2018). “Impacts of the Deepwater Horizon Oil Spill Evaluated Using an End-to-End Ecosystem Model”. In: *PLoS ONE* 13.1. DOI: 10.1371/journal.pone.0190840.

Beal, Lisa M et al. (2015). “Capturing the transport variability of a western boundary jet: Results from the Agulhas Current Time-Series Experiment (ACT)”. In: *Journal of Physical Oceanography* 45.5, pp. 1302–1324. DOI: 10.1175/JPO-D-14-0119.1.

Berenshtein, Igal et al. (Feb. 2020). “Invisible Oil beyond the *Deepwater Horizon* Satellite Footprint”. In: *Science Advances* 6.7, eaaw8863. ISSN: 2375-2548. DOI: 10.1126/sciadv.aaw8863.

Bracco, Annalisa et al. (Sept. 2020). “Transport, Fate and Impacts of the Deep Plume of Petroleum Hydrocarbons Formed During the Macondo Blowout”. In: *Frontiers in Marine Science* 7, p. 542147. ISSN: 2296-7745. DOI: 10.3389/fmars.2020.542147.

Brandvik, Per Johan et al. (Feb. 2021). “Large-Scale Basin Testing to Simulate Realistic Oil Droplet Distributions from Subsea Release of Oil and the Effect of Subsea Dispersant Injection”. In: *Marine Pollution Bulletin* 163, p. 111934. ISSN: 0025326X. DOI: 10.1016/j.marpolbul.2020.111934.

Bryden, Harry L, Lisa M Beal, and Louise M Duncan (2005). “Structure and transport of the Agulhas Current and its temporal variability”. In: *Journal of Oceanography* 61.3, pp. 479–492.

Chen, Fanghui and Poojitha D. Yapa (Feb. 2007). “Estimating the Oil Droplet Size Distributions in Deepwater Oil Spills”. In: *Journal of Hydraulic Engineering* 133.2, pp. 197–207. DOI: 10.1061/(ASCE)0733-9429(2007)133:2(197).

Dagestad, Knut-Frode et al. (Apr. 2018). “OpenDrift v1.0: A Generic Framework for Trajectory Modelling”. In: *Geoscientific Model Development* 11.4, pp. 1405–1420. ISSN: 1991-9603. DOI: 10.5194/gmd-11-1405-2018.

Debreu, Laurent et al. (2012). “Two-way nesting in split-explicit ocean models: Algorithms, implementation and validation”. In: *Ocean Modelling* 49, pp. 1–21.

ERM (2018). *Environmental Impact Assessment for Proposed Exploration Drilling in Block ER 236, Offshore of Kwa-Zulu Natal Coast of South Africa – Oil Spill Modelling Report*.

Etkin, Dagmar (2015). “Offshore Well Blowout Probability Model”. In: *Proceedings of the 38th Arctic and Marine Oilspill Program Technical Seminar on Environmental Contamination and Response*.

French, D. et al. (1996). *The CERCLA Type A Natural Resource Damage Assessment Model for Coastal and Marine Environments (NRDAM/CME), Technical Documentation, Vol. I-V.*

French-McCay, Deborah P. (2004). “OIL SPILL IMPACT MODELING: DEVELOPMENT AND VALIDATION”. In: *Environmental Toxicology and Chemistry* 23.10, p. 2441. ISSN: 0730-7268, 1552-8618. DOI: 10.1897/03-382.

French-McCay, Deborah P. et al. (Oct. 2021a). “Oil Fate and Mass Balance for the Deepwater Horizon Oil Spill”. In: *Marine Pollution Bulletin* 171, p. 112681. ISSN: 0025326X. DOI: 10.1016/j.marpolbul.2021.112681.

French-McCay, Deborah P. et al. (Dec. 2021b). “Validation of Oil Fate and Mass Balance for the Deepwater Horizon Oil Spill: Evaluation of Water Column Partitioning”. In: *Marine Pollution Bulletin* 173, p. 113064. ISSN: 0025326X. DOI: 10.1016/j.marpolbul.2021.113064.

Gundlach, Erich R. (Apr. 1987). “OIL-HOLDING CAPACITIES AND REMOVAL COEFFICIENTS FOR DIFFERENT SHORELINE TYPES TO COMPUTER SIMULATE SPILLS IN COASTAL WATERS”. In: *International Oil Spill Conference Proceedings* 1987.1, pp. 451–457. ISSN: 2169-3358, 2169-3366. DOI: 10.7901/2169-3358-1987-1-451.

Gurumoorthi, K. et al. (2021). “Fate of MV Wakashio oil spill off Mauritius coast through modelling and remote sensing observations”. In: *Marine Pollution Bulletin* 172, p. 112892. ISSN: 0025-326X. DOI: https://doi.org/10.1016/j.marpolbul.2021.112892. URL: https://www.sciencedirect.com/science/article/pii/S0025326X21009267.

Johansen, Øistein, Per Johan Brandvik, and Umer Farooq (Aug. 2013). “Droplet Breakup in Subsea Oil Releases – Part 2: Predictions of Droplet Size Distributions with and without Injection of Chemical Dispersants”. In: *Marine Pollution Bulletin* 73.1, pp. 327–335. ISSN: 0025326X. DOI: 10.1016/j.marpolbul.2013.04.012.

Krug, M, S Swart, and J Gula (2017). “Submesoscale cyclones in the Agulhas current”. In: *Geophysical Research Letters* 44.1, pp. 346–354.

Lavrenov, I. V. (Mar. 1998). “The Wave Energy Concentration at the Agulhas Current off South Africa”. In: *Natural Hazards* 17.2, pp. 117–127. ISSN: 1573-0840. DOI: 10.1023/A:1007978326982.

Li, Zhengkai, Malcolm L. Spaulding, and Deborah French-McCay (June 2017a). “An Algorithm for Modeling Entrainment and Naturally and Chemically Dispersed Oil Droplet Size Distribution under Surface Breaking Wave Conditions”. In: *Marine Pollution Bulletin* 119.1, pp. 145–152. ISSN: 0025326X. DOI: 10.1016/j.marpolbul.2017.03.048.

Li, Zhengkai et al. (Jan. 2017b). “Development of a Unified Oil Droplet Size Distribution Model with Application to Surface Breaking Waves and Subsea Blowout Releases Considering Dispersant Effects”. In: *Marine Pollution Bulletin* 114.1, pp. 247–257. ISSN: 0025326X. DOI: 10.1016/j.marpolbul.2016.09.008.

Lutjeharms, Johann RE (2006). *The Agulhas current retroflection*. Springer.

Murawski, Steven A. et al., eds. (2020). *Scenarios and Responses to Future Deep Oil Spills: Fighting the Next War*. Cham: Springer International Publishing. ISBN: 978-3-030-12962-0 978-3-030-12963-7. DOI: 10.1007/978-3-030-12963-7.

Ponce de León, Sonia and C. Guedes Soares (Feb. 2021). “Extreme Waves in the Agulhas Current Region Inferred from SAR Wave Spectra and the SWAN Model”. In: *Journal of Marine Science and Engineering* 9.2, p. 153. ISSN: 2077-1312. DOI: 10.3390/jmse9020153.

Preston-Whyte, R. A. (1988). *The atmosphere and weather of southern Africa*. eng. Cape Town: Oxford University Press. ISBN: 0195705149.

Pryor, SC, Grigory Nikulin, and Colin Jones (2012). “Influence of spatial resolution on regional climate model derived wind climates”. In: *Journal of Geophysical Research: Atmospheres* 117.D3.

Pujol, MI and F Mertz (2019). *Sea Level TAC DUACS Products*.

Ragoasha, Natalie et al. (July 2019). “Lagrangian Pathways in the Southern Benguela Upwelling System”. In: *Journal of Marine Systems* 195, pp. 50–66. ISSN: 0924-7963. DOI: 10.1016/j.jmarsys.2019.03.008.

Röhrs, Johannes et al. (Dec. 2018). “The Effect of Vertical Mixing on the Horizontal Drift of Oil Spills”. In: *Ocean Science* 14.6, pp. 1581–1601. ISSN: 1812-0784. DOI: 10.5194/os-14-1581-2018.

Russo, Cristina Serena et al. (2022). “An Intercomparison of Global Reanalysis Products for Southern Africa’s Major Oceanographic Features”. In: *Frontiers in Marine Science*. DOI: 10.3389/fmars.2022.837906.

Schumann, Eckart H., C. Fiona MacKay, and Nadine A. Strydom (May 2019). “Nurdle Drifters around South Africa as Indicators of Ocean Structures and Dispersion”. In: *South African Journal of Science* 115.5/6. ISSN: 1996-7489. DOI: 10.17159/sajs.2019/5372.

Shchepetkin, Alexander F and James C McWilliams (2005). “The regional oceanic modeling system (ROMS): a split-explicit, free-surface, topography-following-coordinate oceanic model”. In: *Ocean modelling* 9.4, pp. 347–404.

Spaulding, Malcolm et al. (July 2017). “Application of an Integrated Blowout Model System, OILMAP DEEP, to the Deepwater Horizon (DWH) Spill”. In: *Marine Pollution Bulletin* 120.1, pp. 37–50. ISSN: 0025-326X. DOI: 10.1016/j.marpolbul.2017.04.043.

Tedesco, P. et al. (Nov. 2019). “Generation of Submesoscale Frontal Eddies in the Agulhas Current”. In: *Journal of Geophysical Research: Oceans* 124.11, pp. 7606–7625. ISSN: 2169-9275, 2169-9291. DOI: 10.1029/2019JC015229.

Tkalich, Pavlo and Eng Soon Chan (Nov. 2002). “Vertical Mixing of Oil Droplets by Breaking Waves”. In: *Marine Pollution Bulletin* 44.11, pp. 1219–1229. ISSN: 0025326X. DOI: 10.1016/S0025-326X(02)00178-9.

Veitch, Jennifer, Pierrick Penven, and Frank Shillington (Sept. 2010). “Modeling Equilibrium Dynamics of the Benguela Current System”. In: *Journal of Physical Oceanography* 40.9, pp. 1942–1964. ISSN: 0022-3670, 1520-0485. DOI: 10.1175/2010JPO4382.1.

Veitch, Jennifer et al. (Dec. 2018). “Shelf-Edge Jet Currents in the Southern Benguela: A Modelling Approach”. In: *Journal of Marine Systems*. Benguela: Opportunity, Challenge and Change 188, pp. 27–38. ISSN: 0924-7963. DOI: 10.1016/j.jmarsys.2017.09.003.

Veitch, Jennifer A. and Pierrick Penven (2017). “The Role of the Agulhas in the Benguela Current System: A Numerical Modeling Approach”. In: *Journal of Geophysical Research: Oceans* 122.4, pp. 3375–3393. ISSN: 2169-9291. DOI: 10.1002/2016JC012247.

Vermeulen, Estee Ann et al. (2019). “Investigating the relationship between volume transport and sea surface height in a numerical ocean model”. In: *Ocean Science* 15.3, pp. 513–526. DOI: 10.5194/os-2018-117.

Wu, Jin (Aug. 1983). “Sea-Surface Drift Currents Induced by Wind and Waves”. In: *Journal of Physical Oceanography* 13.8, pp. 1441–1451. ISSN: 0022-3670, 1520-0485. DOI: 10.1175/1520-0485(1983)013<1441:SSDCIB>2.0.CO;2.

Zhao, Lin et al. (July 2017). “Droplet and Bubble Formation of Combined Oil and Gas Releases in Subsea Blowouts”. In: *Marine Pollution Bulletin* 120.1-2, pp. 203–216. ISSN: 0025326X. DOI: 10.1016/j.marpolbul.2017.05.010.